ANL-NE-08/25

Argonne NATIONAL LABORATORY

Target Design Optimization for an Electron Accelerator Driven Subcritical Facility with Circular and Square Beam Profiles

Nuclear Engineering Division

About Argonne National Laboratory

Argonne is a U.S. Department of Energy laboratory managed by UChicago Argonne, LLC under contract DE-AC02-06CH11357. The Laboratory's main facility is outside Chicago, at 9700 South Cass Avenue, Argonne, Illinois 60439. For information about Argonne, see www.anl.gov.

Availability of This Report

This report is available, at no cost, at http://www.osti.gov/bridge. It is also available on paper from the U.S. Department of Energy and its contractors, for a processing fee, from:

U.S. Department of Energy
Office of Scientific and Technical Information
P.O. Box 62
Oak Ridge, TN 37831-0062
phone (865) 576-8401
fax (865) 576-5728
reports@adonis.osti.gov

ANL-NE-08/25

Target Desgin Optimization for an Electron Accelerator Driven Subcritical Facility with Circular and Square Beam Profiles

by
Tanju Sofu, Yousry Gohar, Zhaopeng Zhong, Henry Belch, and Dmitry Naberezhnev
Nuclear Engineering Division, Argonne National Laboratory

August 2008

UChicago ▶ Argonne LLC

Office of Science
U.S. DEPARTMENT OF ENERGY

A U.S. Department of Energy laboratory managed by UChicago Argonne, LLC

Target Design Optimization for an Electron Accelerator Driven Subcritical Facility with Circular and Square Beam Profiles

Table of Contents

Target Design Optimization for an Electron Accelerator Driven Subcritical Facility with Circular and Square Beam Profiles

List of Figures

Target Design Optimization for an Electron Accelerator Driven Subcritical Facility with Circular and Square Beam Profiles

List of Tables

Target Design Optimization for an Electron Accelerator Driven Subcritical Facility with Circular and Square Beam Profiles

Executive Summary

A subcritical facility driven by an electron accelerator is planned at the Kharkov Institute of Physics and Technology (KIPT) in Ukraine for medical isotope production, materials research, training, and education. The conceptual design of the facility is being pursued through collaborations between ANL and KIPT.[1-4] As part of the design effort, the high-fidelity analyses of various target options are performed with formulations to reflect the realistic configuration and the three dimensional geometry of each design.[5-7] This report summarizes the results of target design optimization studies for electron beams with two different beam profiles.

The target design optimization is performed via the sequential neutronic, thermal-hydraulic, and structural analyses for a comprehensive assessment of each configuration. First, a target CAD model is developed with proper emphasis on manufacturability to provide a basis for separate but consistent models for subsequent neutronic, thermal-hydraulic, and structural analyses. The optimizations are pursued for maximizing the neutron yield, streamlining the flow field to avoid hotspots, and minimizing the thermal stresses to increase the durability. In addition to general geometric modifications, the inlet/outlet channel configurations, target plate partitioning schemes, flow manipulations and rates, electron beam diameter/width options, and cladding material choices are included in the design optimizations.

The electron beam interactions with the target assembly and the neutronic response of the subcritical facility are evaluated using the MCNPX code.[8] The results for the electron beam energy deposition, neutron generation, and utilization in the subcritical pile are then used to characterize the axisymmetric heat generation profiles in the target assembly with explicit simulations of the beam tube, the coolant, the clad, and the target materials. Both tungsten and uranium are considered as target materials. Neutron spectra from tungsten and uranium are very similar allowing the use of either material in the subcritical assembly without changing its

characteristics. However, the uranium target has a higher neutron yield, which increases the neutron flux of the subcritical assembly.

Based on the considered dimensions and heat generation profiles, the commercial CFD software Star-CD[9] is used for the thermal-hydraulic analysis of each target design to satisfy a set of thermal criteria, the most limiting of which being to maintain the water temperature 50°C below the boiling point. It is found that the turbulence in the inlet channels dissipates quickly in narrow gaps between the target plates and, as a result, the heat transfer is limited by the laminar flow conditions. On average, 3-D CFD analyses of target assemblies agree well with 1-D calculations using RELAP (performed by KIPT). However, the recirculation and stagnation zones predicted with the CFD models prove the importance of a 3-D analysis to avoid the resulting hotspots.

The calculated temperatures are subsequently used for the structural analysis of each target configuration to satisfy the other engineering design requirements. The thermo-structural calculations are performed mostly with NASTRAN and the results occasionally compared with the results from MARC. Both, NASTRAN and MARC are commercially available structural-mechanics analysis software.[10] Although, a significant thermal gradient forms in target elements along the beam direction, the high thermal stresses are generally observed peripherally around the edge of thin target disks/plates. Due to its high thermal conductivity, temperatures and thermal stresses in tungsten target are estimated to be significantly lower than in uranium target. The deformations of the target disks/plates are found to be insignificant, which eliminate concerns for flow blockages in narrow coolant channels.

Consistent with the specifications of the KIPT accelerator to be used in this facility, the electron beam power is 100-kW with electron energy in the range of 100 to 200 MeV. As expected, the 100 MeV electrons deposit their energy faster while the 200-MeV electrons spread their energy deposition further along the beam direction. However in that electron energy range, the energy deposition profiles near the beam window require very thin target plates/disks to limit the temperatures and thermal stresses.

1. General Description of the Target Assembly for Circular Electron Beam

The conceptual design of the subcritical assembly is based on an array of hexagonal fuel elements with low-enriched uranium oxide in aluminum matrix and clad. Configurations with different number of fuel assemblies are analyzed using different combinations of target designs and reflector materials. In each configuration, the seven fuel assemblies at the center of the subcritical pile are replaced with the electron target as shown in Fig. 1-1. The length of the fuel assemblies is 50 cm while the length of the electron target is in the range of 8 to 10 cm depending on the target material and the partitioning scheme. The target assembly is placed vertically at the center of the subcritical assembly.

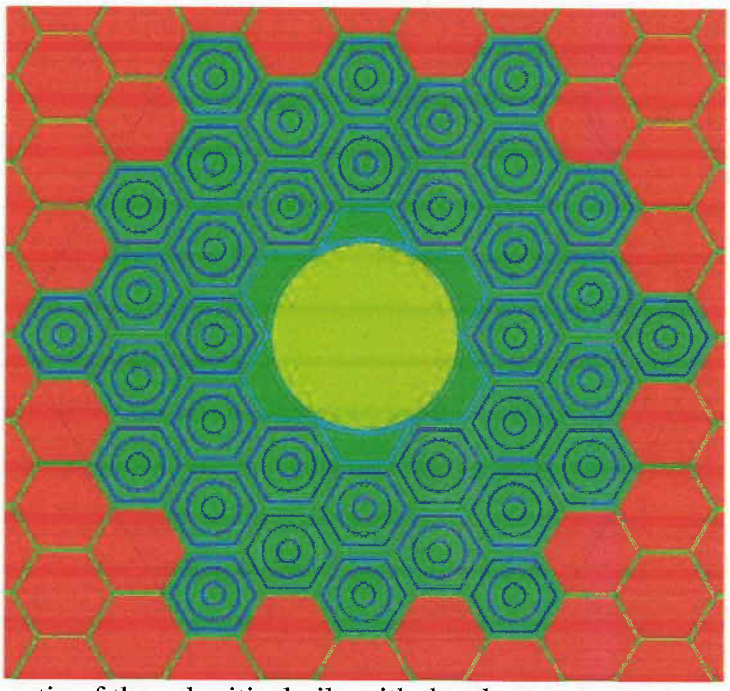

Figure 1-1. Schematic of the subcritical pile with the electron target assembly at the center

Initially, a radially and azimuthally uniform electron beam with circular profile is considered. For the fuel assembly pitch of 3.5 cm, the largest beam diameter that can fit into the yellow circular profile in Fig. 1-1 is estimated as 7.6 cm. The surrounding six half hexagons around the beam tube and target assembly are considered for target coolant inlet and outlet channels (shown in green in Fig. 1-1) and optionally for instrumentation.

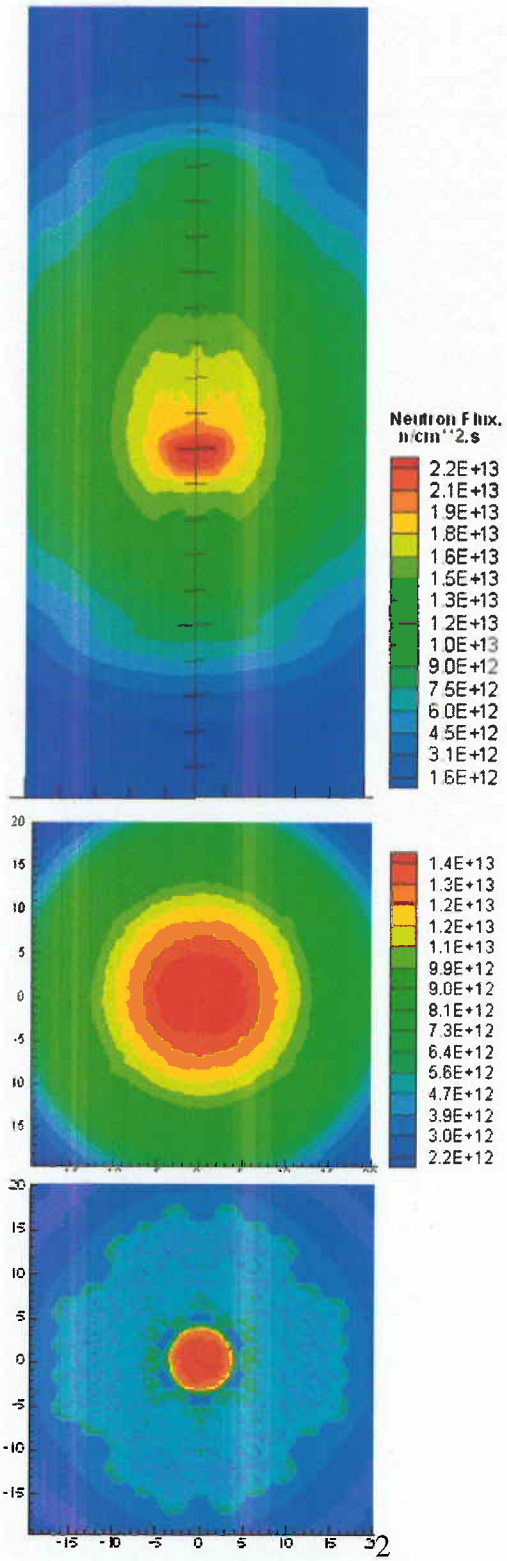

Figure 1-2. Typical axial (top) and radial (middle) neutron flux profiles, and power density distribution (bottom) for a subcritical pile with 74 low-enriched (3-g/cm^3 density) uranium fuel assemblies, water reflector and tungsten target

When the electrons interact with target material, they generate neutrons that drive the subcritical assembly, yielding a neutron flux with typical axial and radial (mid-plane) profiles as shown in top two graphs of Fig. 1-2. The MCNPX computer code is used with continuous energy data libraries and S(α,β) data to analyze the system multiplication factor, neutron flux profiles, and average neutron flux in the irradiation channels.

The power density distribution in the sub-critical assembly is also evaluated with MCNPX. A typical radial power density profile at the mid-plane is shown in the bottom graph of Fig. 1-2. Due to the dissipation of the electron beam as well as the resulting neutron yield in the subcritical assembly, the power density is significantly higher in target assembly (red zone in the bottom graph of Fig. 1-2) in comparison to neighboring fuel assemblies, requiring a separate cooling system to meet the set of thermo-mechanical design criteria.

Initially, a radially and azimuthally uniform power density distribution is assumed only in the target material, the power dissipation in the coolant and clad is ignored. The subsequent more detailed assessments with MCNPX code are based on either azimuthally uniform axisymmetric models for the circular electron beam, or full 3-D models for square electron beam to characterize the power density profiles in the different materials of the target assembly.

In each target configuration studied, the coolant with room temperature water coolant flows parallel to the electron beam on one side of the target assembly in parallel channels, splits among narrow gaps between the target disks to cool them, and returns in opposite direction to the beam on other side of the disks. The direction of flow is downward in the inlet channels, and upward in the outlet channels. Such a configuration with two inlet and two outlet channels is shown in Fig. 1-3 for the circular target disks and electron beam profile. Various target plate and coolant channel thicknesses are evaluated and optimal neutron yield, consistent with the needs for proper cooling and structural stability, is obtained with nominally 1.75 mm narrow coolant channels between target disks/plates.

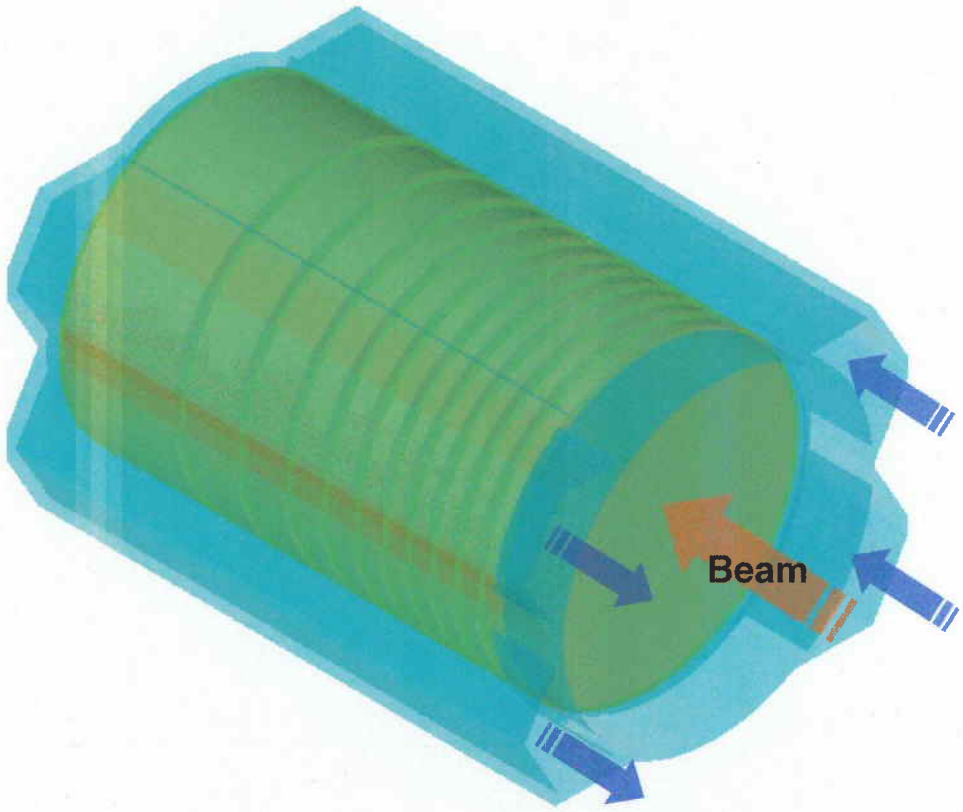

Figure 1-3. The target assembly sketch of the electron beam with circular profile, configuration with two inlet and two outlet channels

In the 100-200 MeV electron energy range, the peak energy deposition takes place near the beam window for tungsten and uranium targets. This requires thin partitioning of the first several target disks/plates to limit the temperatures and resulting thermal stresses. Due to its high thermal conductivity, the calculated temperatures and thermal stresses in tungsten target elements

are significantly lower than the corresponding values for uranium target elements. Although the neutron spectra from tungsten and uranium targets are quite similar, the higher neutron yield of uranium target is more desirable since it increases substantially the neutron flux in the subcritical assembly. Therefore, a greater emphasis is placed on the optimization of the uranium target configurations. The uranium disks are considered to be covered with 0.7 mm thick Aluminum-alloy cladding to avoid coolant contamination with fission products.

The main target thermal performance criteria considered are:

- All solid material temperatures are below 0.8 of their respective melting point.
- The peak water temperature is 50°C below the boiling point (150°C at 4 atm).

The main structural performance criterion has been to keep peak thermal stresses below the yield point of the corresponding material; ~200 MPa is the target for the uranium target material.

For all geometric and flow configurations considered of this study, the average difference between the inlet and outlet water coolant temperatures is less than 5°C. Because of high coolant velocity in the inlet and outlet coolant channels, in the range of 8 to 12 m/s, a fully developed turbulent flow is expected in the inlet channels. However, the turbulence in the flow is estimated to dissipate quickly in the narrow gaps between the target disks/plates, resulting in a laminar heat transfer regime limiting the cooling of the target elements. Also, the recirculation and stagnation zones are anticipated to result in some hotspots, further complicating the thermal and structural design of the target assembly configurations.

The summary of the analyzed target configurations is provided in Tables 1-1 and 1-2 for circular and square target configurations, respectively. The "portioning scheme" in these tables refers to the number of target plates/disks considered in the study and each scheme is identified by a "mod number." For each portioning scheme, several target plate/disk arrangements are studied, each case identified with a "configuration number" and the corresponding unique target disk and coolant gap thicknesses are provided in the body of this report. The main feature(s) of each configuration is listed under the "comments" column. The detailed results (flow field, temperature, and stress distributions) are provided in the attached CD for each case.

Table 1-1. Summary of target configurations studied for electron beam with circular profile, detailed results are given in the CD

Target Material	Heat Load	Partitioning scheme	Conf. #	Detailed Results	Comments
Tungsten	Radially and azimuthally uniform	Mod-1 (7 disks)	1		Reference Design: Uniform heat load in each disk
			2	/circular/Wmod1conf2.ppt	Wider coolant gaps
			3	/circular/Wmod1conf3.ppt	Thinner target disks
		Mod-2 (8 disks)	1	/circular/Wmod2conf1	Adiabatic boundaries, refined grid
			2	/circular/Wmod2conf2	Convective boundaries; refined grid
			3	/circular/Wmod2conf3	Final circular tungsten disk configuration
Al-clad Uranium	Radially and azimuthally uniform	Mod-1 (8 disks)		/circular/Umod1.ppt	Reference design: Uniform heat load in each disk
		Mod-2 (9 disks)	1	/circular/Umod2conf1.ppt	Adiabatic boundaries
			2	/circular/Umod2conf2	Convective boundaries
		Mod-3 (10 disks)	1	/circular/Umod3conf1	Variations on disk thicknesses
			2	/circular/Umod3conf2	Variations on disk thicknesses
			3	/circular/Umod3conf3	Variations on disk thicknesses
			4	/circular/Umod3conf4	Variations on disk thicknesses
		Mod-4	1	/circular/Umod4conf1	Final circular U config. with uniform heat load
	Radially non-uniform	Mod-4 (11 disks)	2	/circular/Umod4conf2	Radially and axially varying heat load
			3	/circular/Umod4conf3	Increased flow rate
			4	/circular/Umod4conf4	Modified mesh with all hexahedral cells
			5	/circular/Umod4conf5	Streamlined channel geometry
			6	/circular/Umod4conf6	Three-inlet and three-outlet channels
			7	/circular/Umod4conf7	Sharp edge channels to minimize stagnation
			8	/circular/Umod4conf8	With peripheral gap between U and Al clad
			9	/circular/Umod4conf9	Non-uniform flow among inlet channels
			10	/circular/Umod4conf10	Thinner second and third target disks
			11	/circular/Umod4conf11	U-238 target
			12	/circular/Umod4conf12	Smaller diameter target
			13	/circular/Umod4conf13	Smaller diameter U-238 target
			14	/circular/Umod4conf14	Larger beam diameter
			15	/circular/Umod4conf15	Larger beam diameter and altered inlet/outlet
			16	/circular/Umod4conf16	Altered inlet/outlet and non-uniform flow
			17	/circular/Umod4conf17	Larger beam diameter and peripheral U-Al gap
			18	/circular/Umod4conf18	Larger beam diameter and peripheral rut
			19	/circular/Umod4conf19	Larger beam diameter and insulated corner

Table 1-2. Summary of target configurations studied for electron beam with square profile, detailed results are given in the CD

Target Material	Heat Load	Partitioning scheme	Conf. #	Detailed Results	Comments
Al-clad Uranium	Full 3-D	Mod-1 (11 disks)	1	/square/Umod1conf1	Coarse grid
			2	/square/Umod1conf2	Refined grid
			3	/square/Umod1conf3	Channel separator removed
			4	/square/Umod1conf4	Higher flow rate
			5	/square/Umod1conf5	Smaller U target cross section
			6	/square/Umod1conf6	Smaller U cross section and peripheral U-Al gap
			7	/square/Umod1conf7	Turbulence inducing ribs
			8	/square/Umod1conf8	Larger beam cross section area
			9	/square/Umod1conf9	Larger beam cross section and peripheral U-Al gap
			10	/square/Umod1conf10	Reduced uranium thicknesses in first six plates
			11	/square/Umod1conf11	Higher flow rate
			12	/square/Umod1conf12	Peripheral U-Al gap
			13	/square/Umod1conf13	Readjusted plate thicknesses
			14	/square/Umod1conf14	Lower flow rate
			15	/square/Umod1conf15	Peripheral U-Al gap only for thin plates
		Mod-2 (12 disks)	1	/square/Umod2conf1	12 plate partitioning scheme
			2	/square/Umod2conf2	Final configuration

2. Results for Circular Electron Beam Profile and Target Disks

Initially, the azimuthally uniform electron beams with circular profiles are considered for the target disk configurations similar to Fig. 1.3. A cutaway of exploded view of the target assembly for the circular target plate configurations is shown in Fig. 2.1. The heat deposition distributions for circular beam are obtained using axisymmetric MCNPX models for both tungsten and uranium target disks.

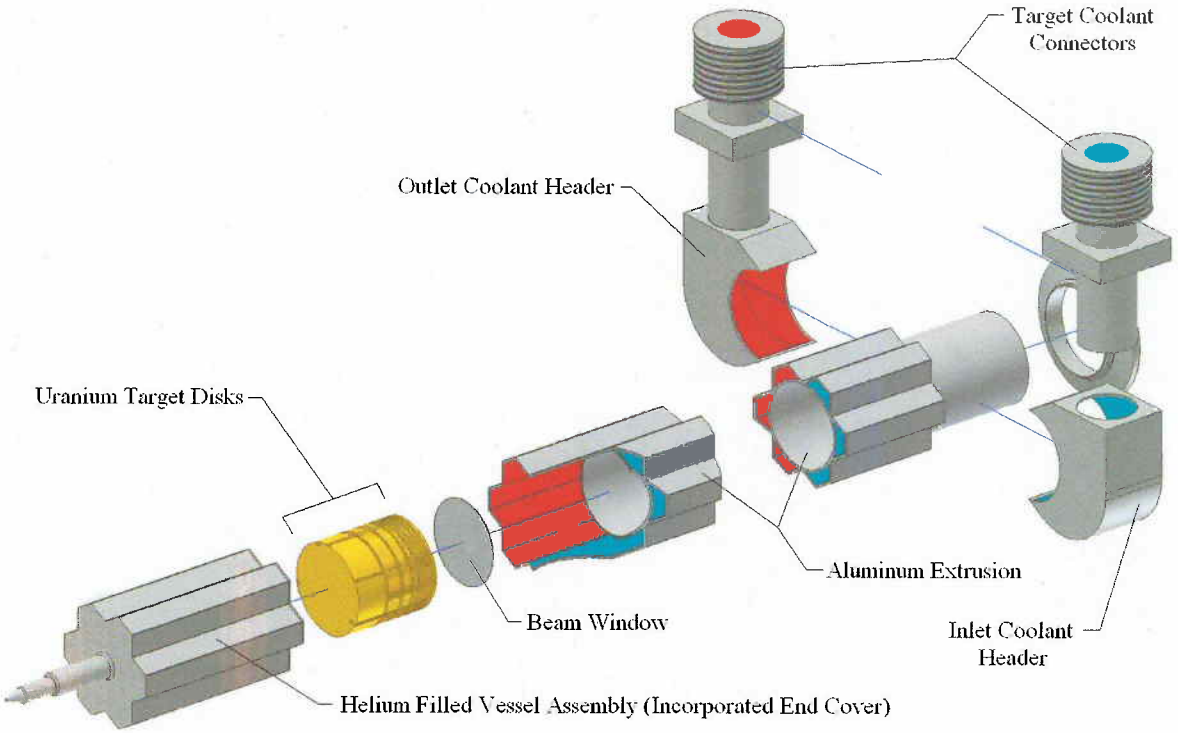

Figure 2-1. Exploded target assembly cutaway for an electron beam with circular cross section

2-1. Tungsten Targets

For all of the tungsten target analyses, a radially and azimuthally uniform heat load is assumed as a function of axial distance along the beam direction as shown in Fig. 2-2. Only two inlet channels and two outlet channels (on the opposite sides) are considered similar to the configuration shown in Figs. 1-1 and 1-3. The remaining two half-hexagonal channels are left open for instrumentation. In each case, the electron beam diameter and the target disk diameter are assumed to be equal to the beam tube inner diameter (77 mm).

Several target partitioning schemes are studied to optimize the heat load distribution, and resulting disk temperatures and stresses in each target plate. Initially a seven-disk partitioning scheme is considered as the reference design to achieve a uniform heat load in each target disk with equal 1.75 mm gap thickness between all seven target disks, after the beam tube window, and before the end plate. However, the results for this reference scheme indicated excessive temperatures for the first several disks suggesting smaller disk thicknesses.

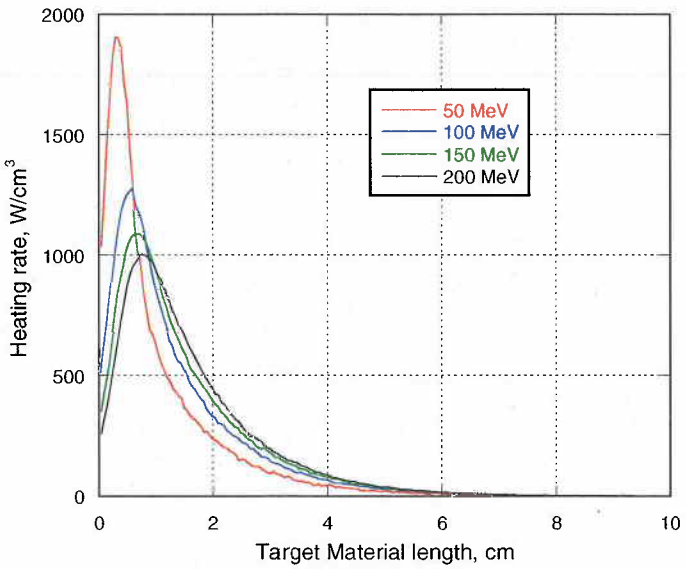

Figure 2-2. Radially and azimuthally uniform heat load as a function of axial distance in tungsten target.

As a result, another seven-disk portioning scheme is also evaluated with reduced thicknesses for the first six target disks and widened coolant gap thicknesses (up to 4 mm) for the first four channels. However, the increased gap thickness did not change turbulence characteristics in the channels between the target plates. Furthermore, adjusting the gap thickness did not alter the flow redistribution between the channels (front to back) significantly. Reducing the plate thicknesses is found to be beneficial but the temperatures near the fourth disk surface reached the coolant boiling point. After several iterations on varying plate/gap thicknesses, grid sensitivity studies, and tightening the convergence criteria, another seven-disk tungsten target configuration with the gap sizes and plate thicknesses shown in Table 2-1 has been identified as the optimal configuration that satisfy the thermal design criteria.

Table 2-1. Target partitioning scheme with seven tungsten disks in third configuration

Coolant channel #	Gap thickness (mm)
1	1
2	2
3	2
4	2
5	2
6	2
7	2
8	1
Total	14

Disk #	Target disk thickness (mm)
1	3
2	3
3	3
4	3
5	4
6	9
7	44
Total	69

With the significantly refined CFD grid and tightened convergence criteria, the flow field is found to be much more uniform within and between the channels in comparison to the earlier results for a coarser grid. The velocity vectors in the middle of second coolant channel for the configuration in Table 2-1 is shown in Fig. 2-3. The uniform flow with smaller recirculation zones reduces the peak temperatures at associated hotspots. The calculated target disk temperatures for 100 and 200 MeV electron beams are shown in Fig. 2-4 for this configuration. In the two cases, the target surface temperatures are globally and locally 50°C below the boiling point and the last (thickest) disk experiences the maximum plate temperatures.

Although the configuration in Table 2-1 and Fig. 2.3 with seven target disks satisfies the thermal design criteria, the high temperatures in thickest target disk cause high thermal stresses in excess of yield strength of tungsten metal, especially for 200 MeV electrons. Therefore, another partitioning scheme with eight tungsten disks is also evaluated. In this new scheme, the seventh target disk is split into two separate disks with the remaining target disk and coolant gap thicknesses retained as in the previous case. The resulting target disk temperatures for 100 and 200 MeV electron beams are shown in Fig. 2-5 for this configuration.

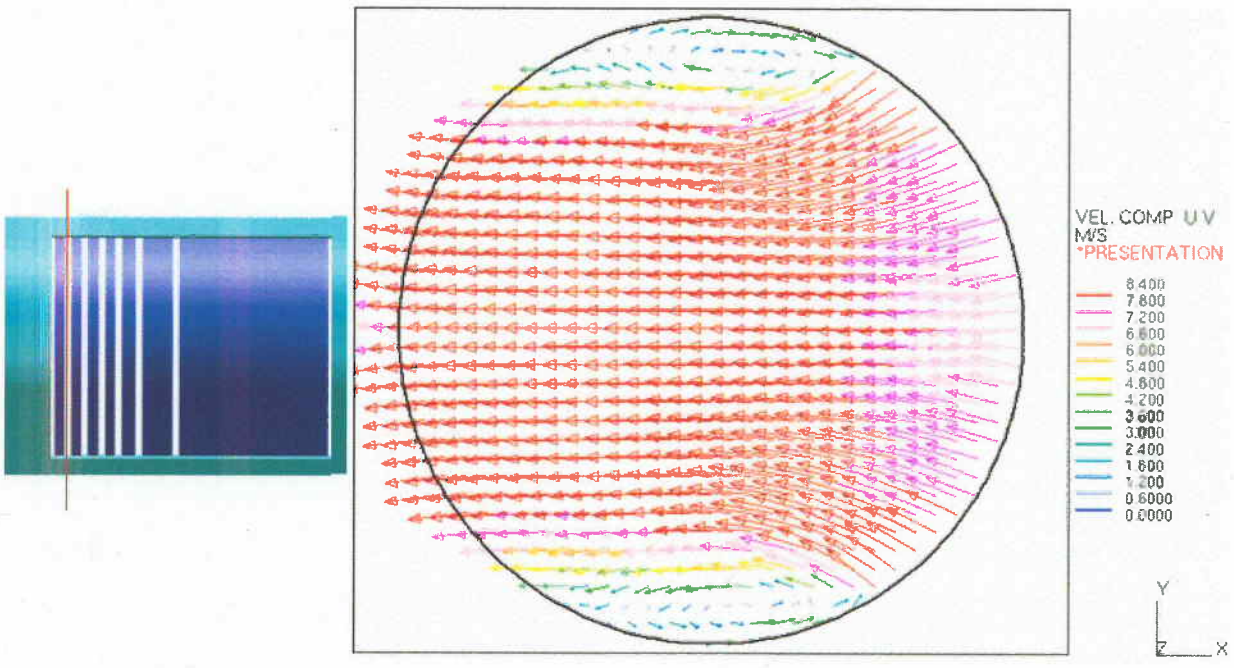

Figure 2-3. Flow field in the middle of coolant channel between first and second target disks for third configuration with seven tungsten target disks, refined grid CFD solutions

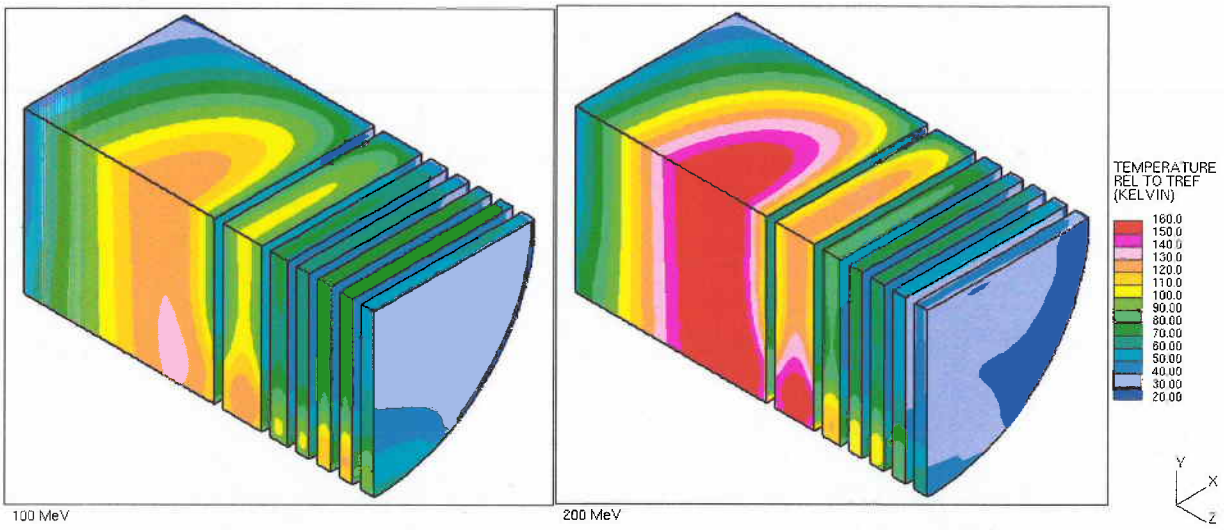

Figure 2- 4 Tungsten target temperatures with 100 MeV (left) and 200 MeV electrons (right) for the partitioning scheme with seven target disks

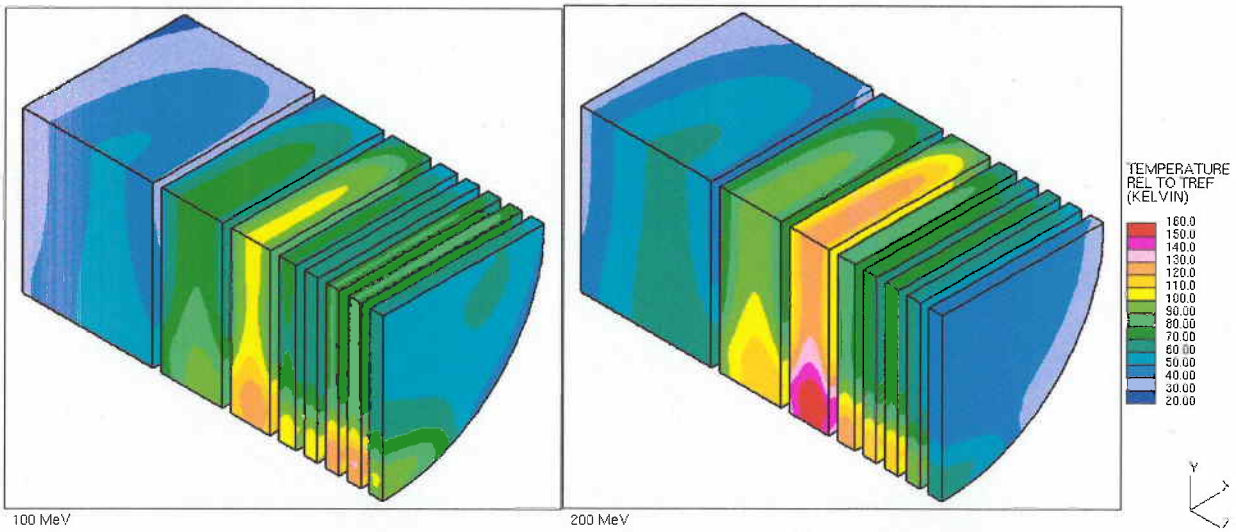

Figure 2-5. Tungsten target temperatures with 100 MeV (left) and 200 MeV electrons (right) for the partitioning scheme with eight target disks

The CFD calculations up to this point considered adiabatic boundary conditions for all external surfaces. Since the electron target will be placed in the middle of the subcritical pile inside a large pool, the external cooling of the target assembly is expected to have an effect on peak temperatures. In order to capture it, the eight-disk configuration in Fig. 2-5 is reevaluated with the external boundaries of the model modified as convective using a rather conservative value for the heat transfer coefficient (10 kW/m^2-K). The updated target disk temperatures with

convective boundary conditions are shown in Fig. 2-6, and they indicate 30K reduction in the peak temperatures. Consequently, for all the analyses that follow, only the convective boundary condition is used.

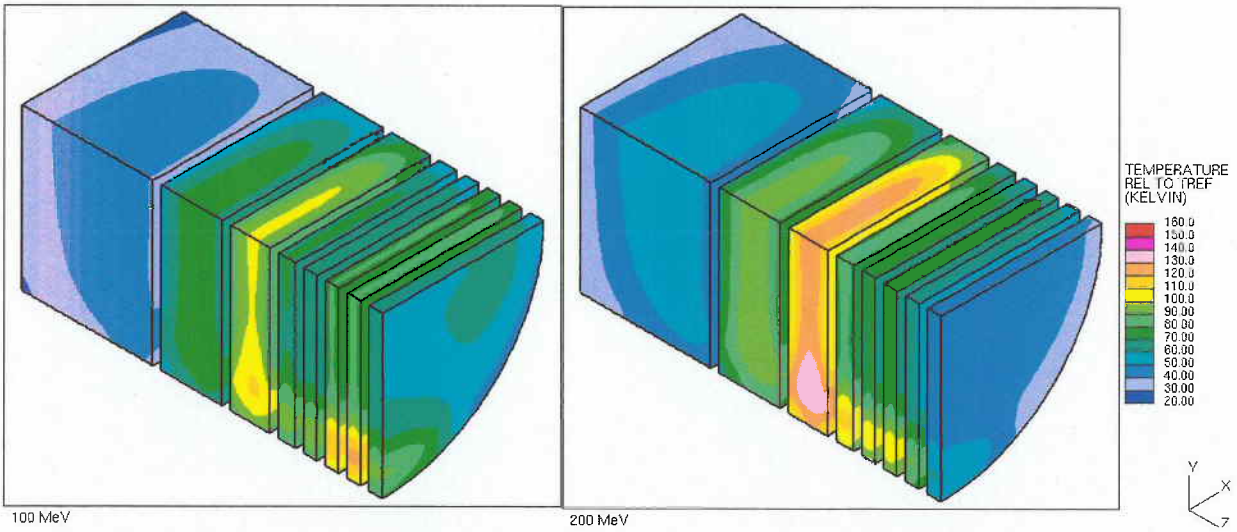

Figure 2-6. Tungsten target temperatures with 100 MeV (left) and 200 MeV electrons (right) for the partitioning scheme with eight target disks with convective boundary.

The temperatures in Fig. 2-6 show that disk number 6 is disproportionately hotter than the other disks particularly for 200 MeV electrons. To avoid it, a final configuration with reduced disk 6 and 7 thicknesses is also studied. The target disk and coolant gap thicknesses for this final circular tungsten target configuration are given in Table 2.2. This new configuration resulted in uniform temperature distribution between all eight disks as shown in Fig. 2-7; therefore it is accepted as the final tungsten target configuration for the electron beam with a circular cross section.

Table 2-2. Target partitioning scheme with eight tungsten disks in third configuration

Coolant channel #	Gap thickness (mm)
1	1.
2	2.
3	2.
4	2.
5	2.
6	2.
7	2.
8	2.
9	1.
Total	16.

Disk #	Target disk thickness (mm)
1	3.0
2	3.0
3	3.0
4	3.0
5	4.0
6	8.0
7	13.0
8	33.0
Total	69.0

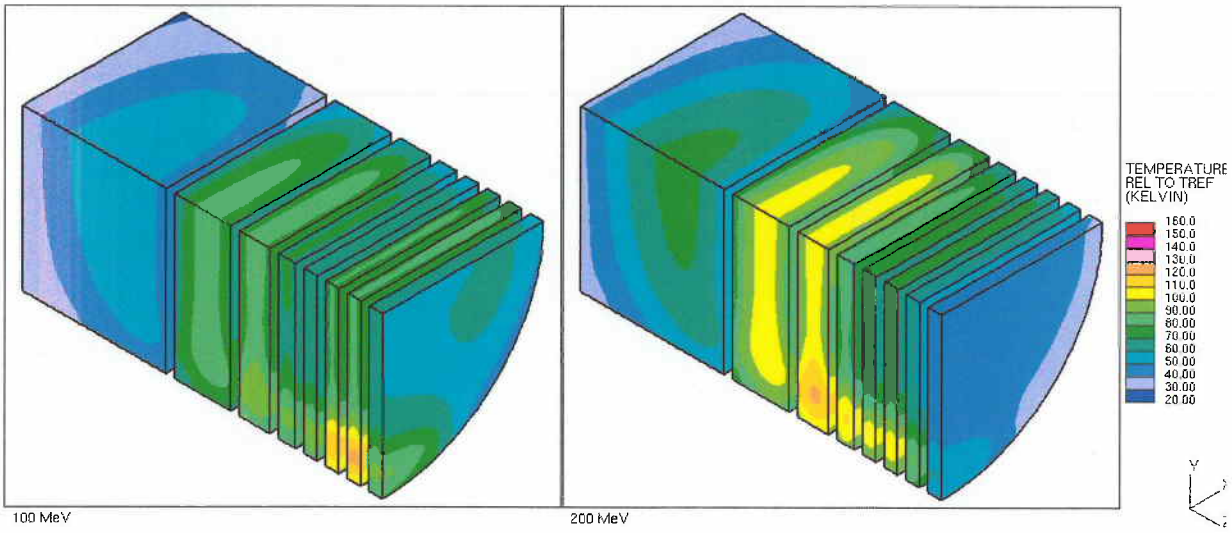

Figure 2- 7.Tungsten target temperatures with 100 MeV (left) and 200 MeV electrons (right) for the partitioning scheme with eight target disks, final configuration

2-2. Al-Clad Uranium Targets with Radially Uniform Heat Load

Similar to the tungsten target cases, initially radially and azimuthally uniform heat load is assumed as a function of axial distance along the beam direction as shown in Fig. 2-8 for the uranium target analyses. Also, two inlet channels and two outlet channels are considered similar to the tungsten target analyses and the configuration shown in Fig. 1-3. The uranium disks are considered with 0.5 mm thick aluminum clad to prevent the coolant contamination with fission products. The electron beam diameter and the target disk diameter are assumed to be equal to the beam tube inner diameter (77 mm).

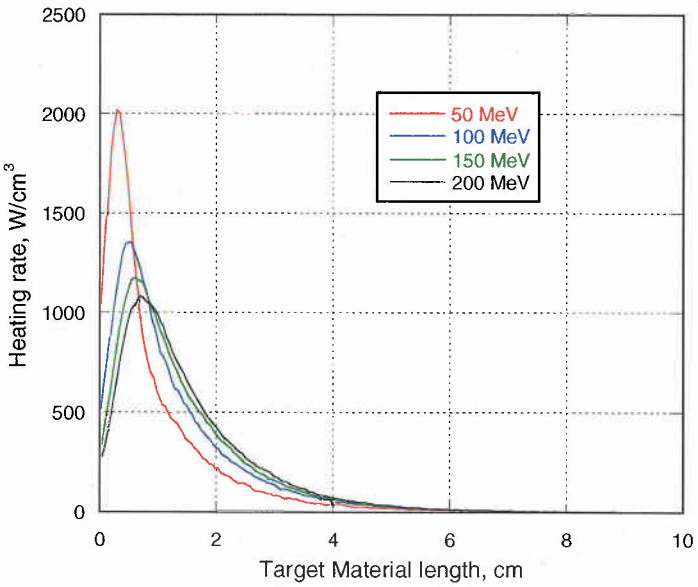

Figure 2-8. Radially and azimuthally uniform heat load as a function of axial distance in tungsten target.

Based on the gained experience with the CFD model for the tungsten target disks, initially an eight-disk partitioning scheme is considered as the reference design with 2-mm gap thickness between the target disks, and 1-mm after the beam tube window and before the end plate. The target disk thicknesses for this reference design are given in Table 2-3. The CFD calculations are pursued using a refined grid and tightened convergence criteria. Consistent with the tungsten target results, the flow field within and between the channels is found to be fairly uniform with velocity vectors similar to what is shown in Fig. 2-3. But due to lower thermal conductivity of uranium, disk number seven temperatures turned out significantly higher than the other disks as shown in Fig.2-9.

Table 2-3. Target partitioning scheme with eight uranium disks

Coolant channel #	Gap thickness (mm)
1	1.
2	2.
3	2.
4	2.
5	2.
6	2.
7.	2.
8	2.
9	1.
Total	16.

Disk #	Target disk thickness (mm)
1	3.0
2	3.0
3	3.0
4	3.0
5	4.0
6	8.0
7	24.0
8	32.5
Total	80.5

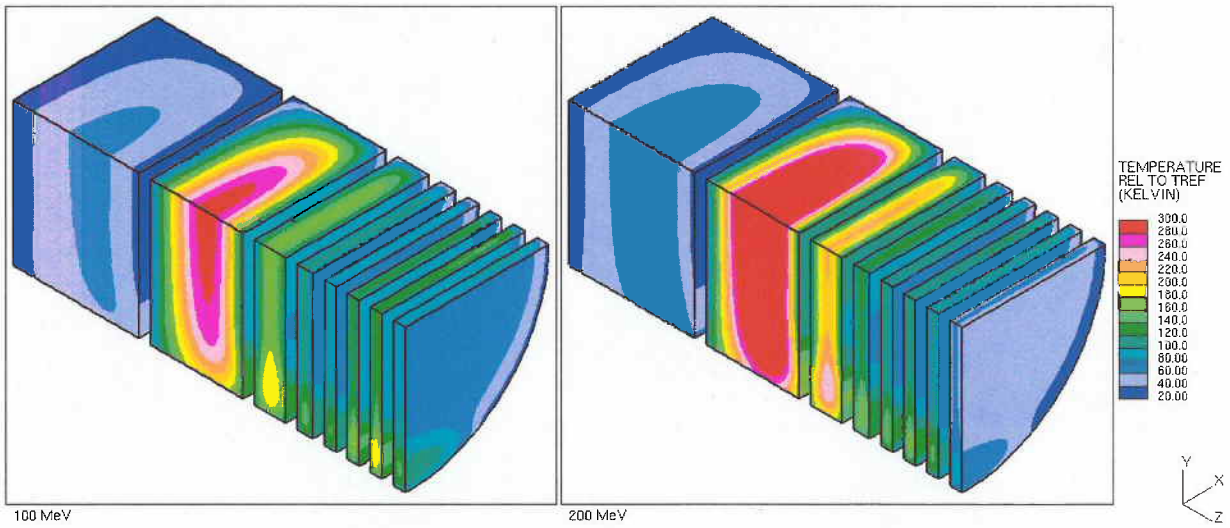

Figure 2-9. Uranium target temperatures with 100 MeV (left) and 200 MeV electrons (right) for a target partitioning scheme with eight disks

To reduce the temperature of the seventh uranium disk, this disk is divided to two, adding another coolant channel into the configuration. The coolant gap and the target disk thicknesses for this partitioning scheme with nine target disks are given in Table 2-4. The additional 2 mm

coolant gap in the active target region is assumed to be tolerable in terms of its effect on the neutron yield and reduced flow rate in other channels. The nine-disk configuration in Table 2-4 is evaluated with both adiabatic and convective boundaries for the external surface. The case with the convective boundaries has specified a contact resistance on external surfaces equivalent of 10-kW/m^2-K for the heat transfer coefficient. For both cases, the target disk temperatures showed a much more uniform distribution and the coolant temperatures at the target disk surfaces satisfied the thermal design criteria to remain at least 50°C below the boiling limit. The peak temperatures were about 20°C lower with the convective external wall boundary conditions, for which the target temperatures are shown in Fig. 2-10. Since, the electron target in the middle of the subcritical pile will be inside a large pool where significant external cooling is expected, the convective boundary conditions are used consistently for all the analyses that follow.

Table 2-4. Target partitioning scheme with nine uranium disks

Coolant channel #	Gap thickness (mm)
1	1.
2	2.
3	2.
4	2.
5	2.
6	2.
7	2.
8	2.
9	2.
10	1.
Total	18.

Disk #	Target disk thickness (mm)
1	3.0
2	3.0
3	3.0
4	3.0
5	4.0
6	6.0
7	8.0
8	14.0
9	36.5
Total	80.5

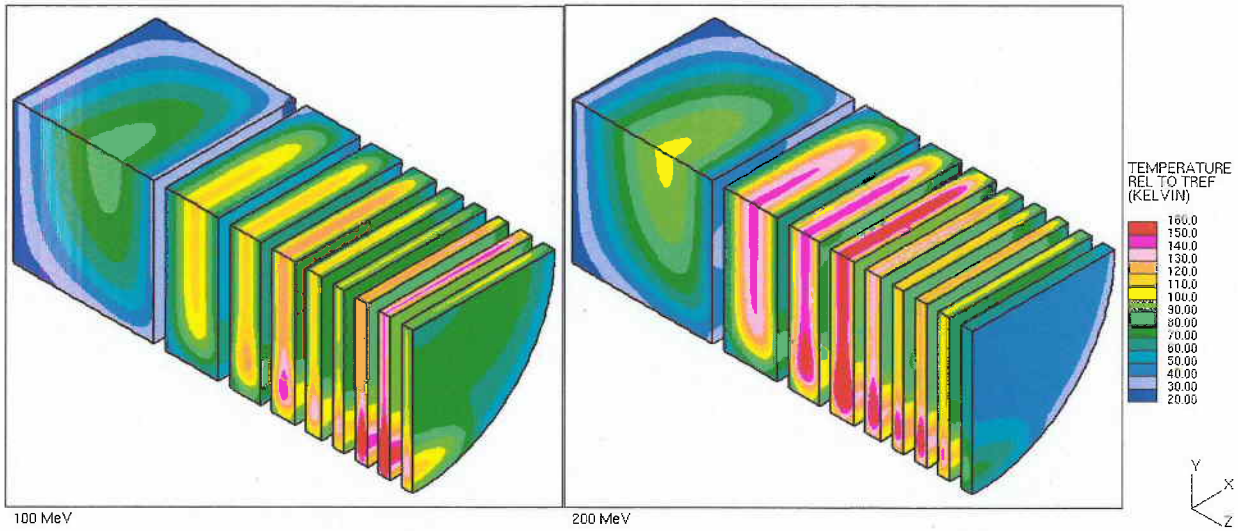

Figure 2-10. Uranium target temperatures with 100 MeV (left) and 200 MeV electrons (right) for a target partitioning scheme with nine disks and convective external boundaries

Even with the convective boundaries, the temperature of the disk number six is disproportionately higher than the other disks for 200 MeV electrons. Also, the target disk surface temperatures near the recirculation zones approach the coolant boiling point. To address these concerns, another partitioning scheme with ten uranium disks is considered next. Four different configurations are studied, each with different set of target disk thicknesses but identical coolant gap thicknesses as summarized in Table 2-5. The corresponding target disk temperatures for each of the four configurations are shown in Fig. 2-11.

Table 2-5. Target partitioning scheme with ten uranium disks

Coolant channel #	Gap thickness (mm)
1	1.
2	2.
3	2.
4	2.
5	2.
6	2.
7	2.
8	2.
9	2.
10	2.
11	1.
Total	18.

Disk #	Target disk thickness (mm)			
	Conf-1	Conf-2	Conf-3	Conf-4
1	3.	3.	3.	3.
2	3.	3.	3.	3.
3	3.	3.	3.	3.
4	3.	3.	3.	3.
5	3.	3.	3.	3.
6	4.	4.	4.	4.
7	5.	5.	5.	5.
8	9.	8.	7.	7.
9	14.	13.	13.	12.
10	32.	34.	35.	36.
Total	79.	79.	79.	79.

For 200 MeV electrons, the calculated Von-Misses stresses in the target disks as a result of thermal gradients are shown in Fig. 2-12 for the configurations with 10 disk portioning scheme. These results suggest thermal stresses in excess of 200 MPa for several target disks in the four configurations. The red color contours in Fig. 2-12 correspond to 259 MPa thermal stress for configuration 1; 228 MPa for configuration 2; 214 MPa for configuration 3; and 211 MPa for configuration 4. It should be noted that Fig. 2.12 shows only the stresses in the uranium target. The estimated stresses in the aluminum clad are negligible. For the 10 disk partitioning scheme, the fourth configuration, configuration-4 Table 2-5, fairly uniform temperature distributions for the ten disks. In addition, this configuration has the lowest thermal stresses with peak values limited to a narrow strips at the peripheral edge of the uranium disks.

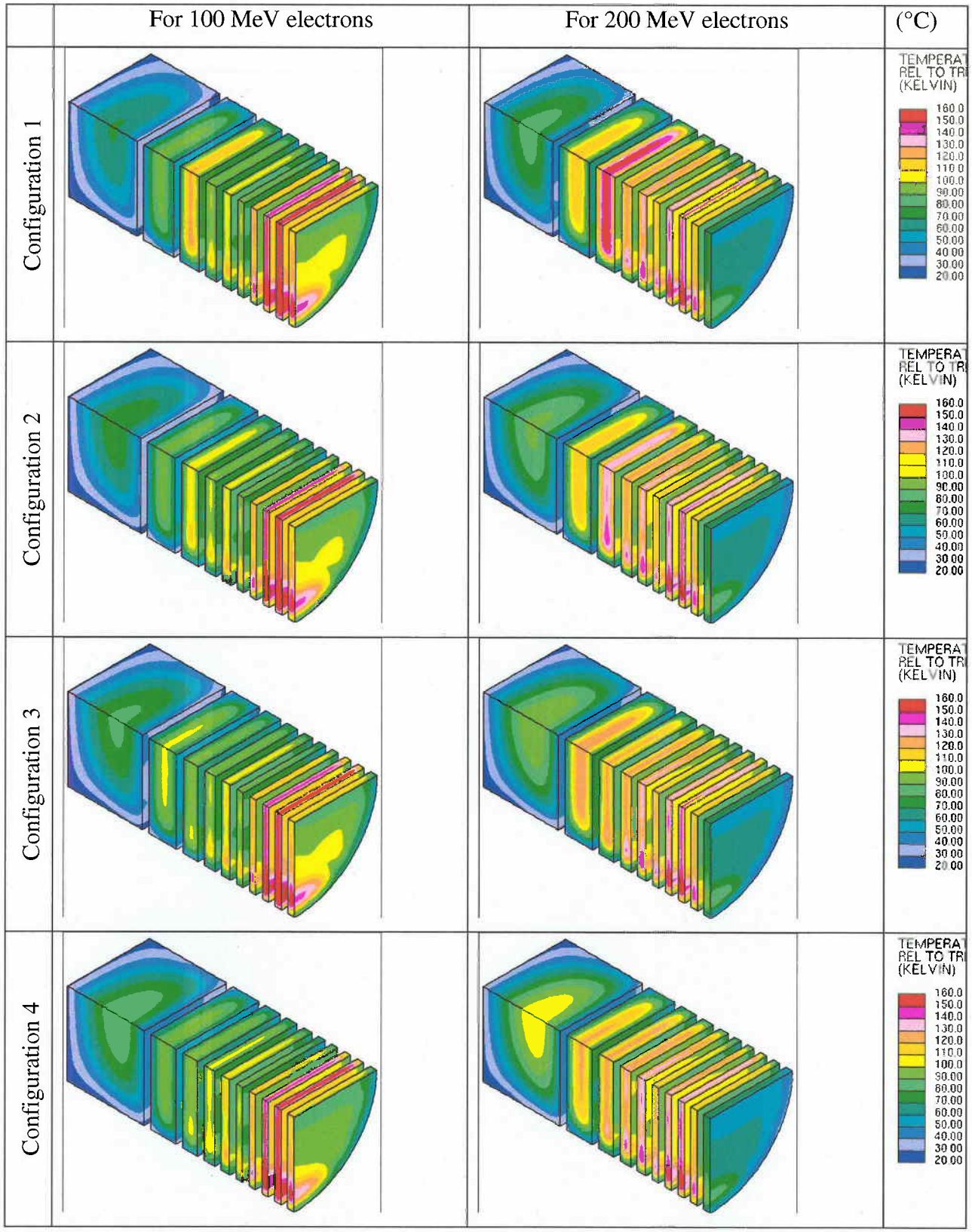

Figure 2-11. Uranium target temperatures with 100 MeV (left) and 200 MeV (right) electrons for the target partitioning scheme with ten disks shown in Table 2-5

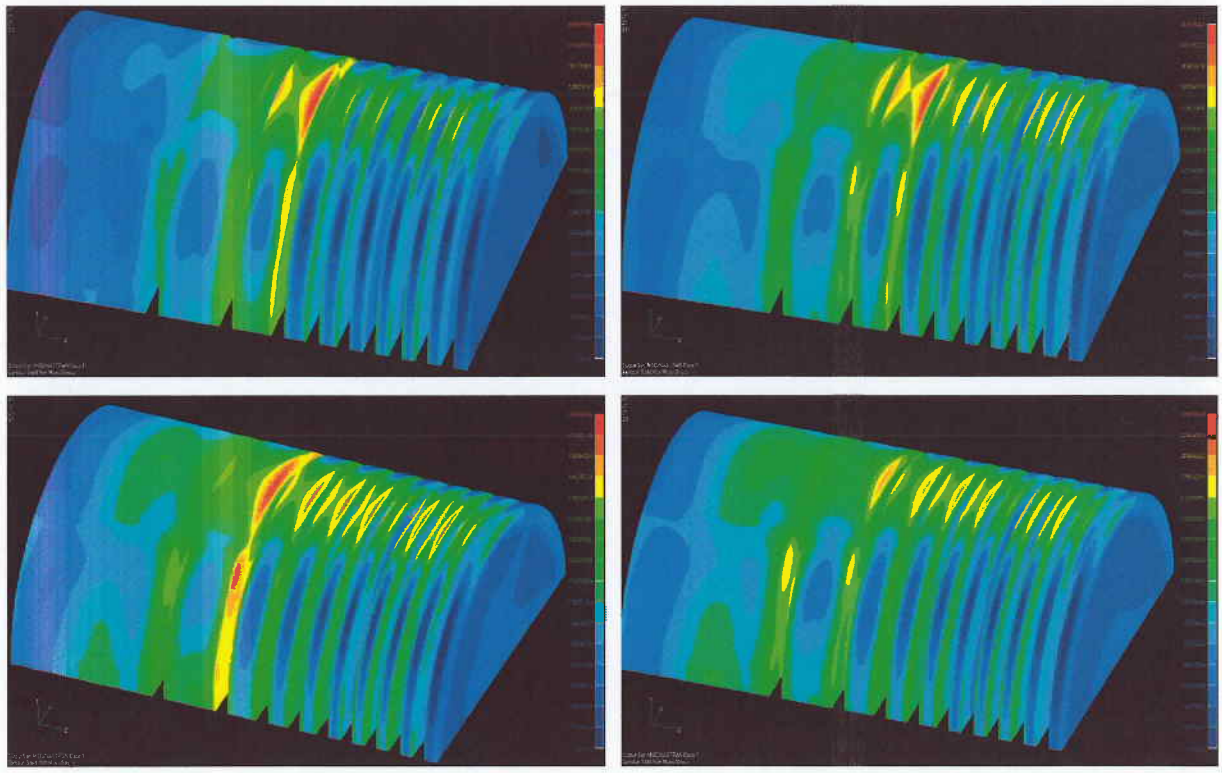

Figure 2-12Calculated Von-Misses stresses in the target disks with 10 disk partitioning scheme for 200 MeV electrons: Configuration 1 (top left), configuration 2 (top right), configuration 3 (bottom left), and configuration 4 (bottom right).

Despite the fact the fourth configuration is fairly close to satisfying the all thermal and structural criteria, a final partitioning scheme with eleven target disks are also considered. The 19 different configurations, boundary conditions, and inlet/outlet distributions are evaluated as summarized in Table 1-1. To minimize the impact of additional coolant gap between the target disks on the neutron yield, the gap thickness is reduced to 1.75 mm in 11 disk partitioning scheme as shown in Table 2-6. With these dimensions, the peak stress was below 200 MPa for 200 MeV electrons.

Table 2-6. Target partitioning scheme with eleven uranium disks

Coolant channel #	Gap thickness (mm)
1	1.75
2	1.75
3	1.75
4	1.75
5	1.75
6	1.75
7	1.75
8	1.75
9	1.75
10	1.75
11	1.75
12	1.75
Total	21.

Disk #	Target disk thickness (mm)
1	3.0
2	3.0
3	3.0
4	3.0
5	3.0
6	4.0
7	5.0
8	6.0
9	9.0
10	12.0
11	28.0
Total	79.0

2-3. Aluminum-Clad Uranium Target Configurations with Axisymmetric Heat Load

The analyses performed up to this point have a radially and azimuthally uniform heat load only as a function of axial distance along the beam direction as shown in Fig. 2-8. For more realistic heat load distribution in the target disks, an axisymmetric MCNPX model is used to provide radially as well as axially varying power density profiles. The first configuration studied with nonuniform heat load is the partitioning scheme shown in Table 2-6. The power density and temperature distributions for both 100 and 200 MeV electrons are shown in Figs 2-13 and 2-14, respectively.

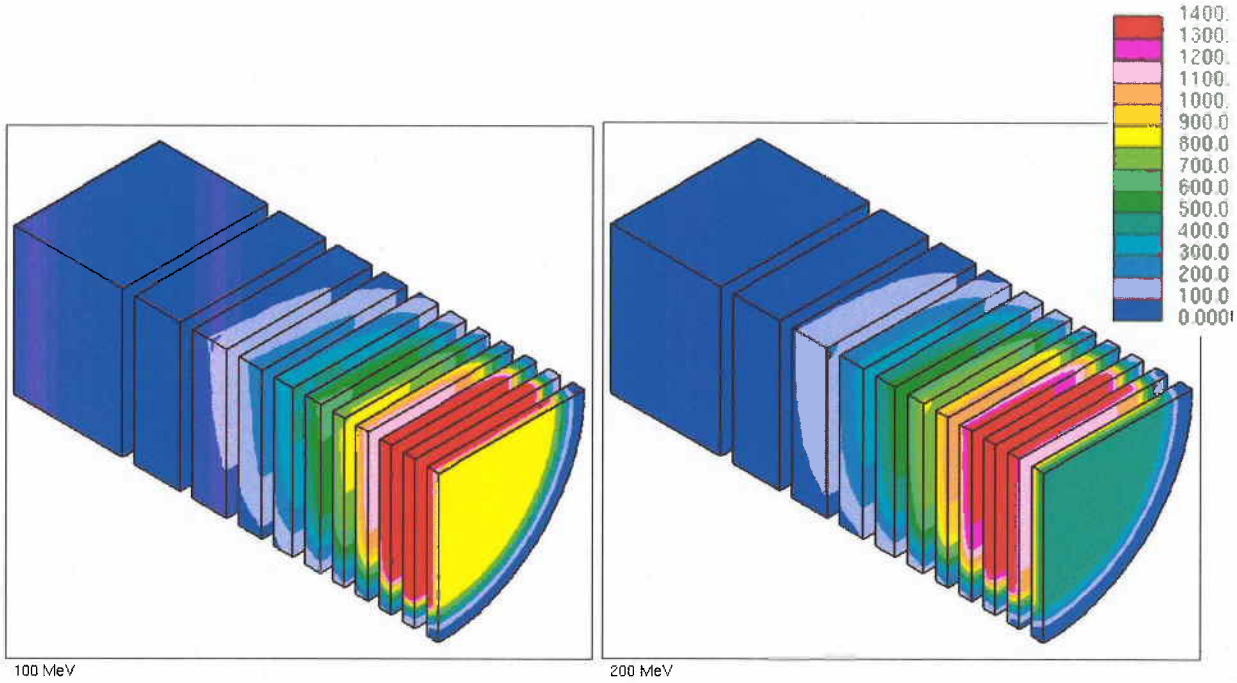

Figure 2-13. Radially and axially varying power density (W/m^3) for 100 MeV (left) and 200 (right) MeV electrons for a partitioning scheme with eleven target disks

Since more heat is deposited around the centerline of the electron beam, the calculated temperatures with non-uniform heat load cases are significantly higher than the earlier analyzed configurations. Furthermore, larger radial temperature gradients cause much greater peripheral stresses, in excess of 500 MPa for the 100 MeV electrons, and 350 MPa for the 200 MeV electrons.

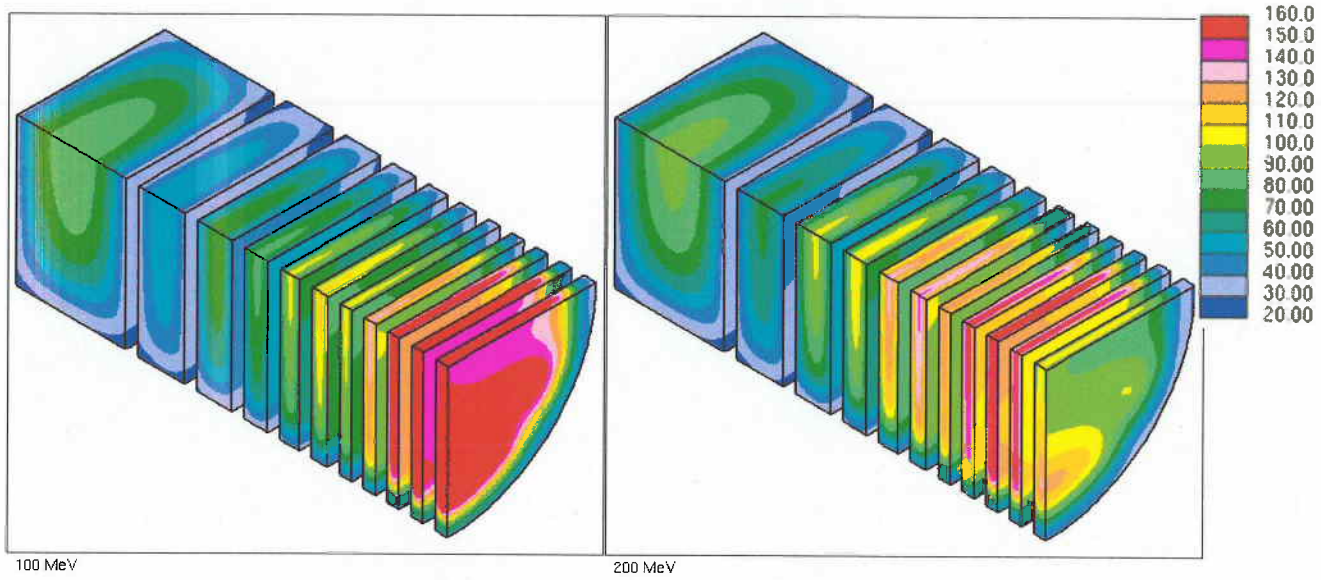

Figure 2-14. Uranium target temperatures (°C) for 100 MeV (left) and 200 MeV (right) electrons for a target partitioning scheme with eleven target disks and non-uniform heat load.

The effect of increasing the flow rate is examined as a part of the optimization studies. About 60% increase in the flow rate increases the nominal inlet channel velocity from 9 m/s to 15 m/s and reduces the peak temperatures. However the peripheral stresses are much higher than the 200 MPa target value, 380 MPa for 100 MeV, and 280 MPa for 200 MeV electrons. The grid sensitivity of the calculated results is evaluated by analyzing the high flow rate case using a different mesh structure with all hexahedral computational cells. The obtained flow and temperatures distributions are consistent with the earlier results, confirming that the grid independent solutions are achieved. Several other configurations are studied using this all-hexahedral mesh structure. But later on, the original mesh structure with collapsed cells along the symmetry line is preferred since it provides a consistent grid with MCNPX calculations and avoids uncertainties in interpolating the proper power density distributions from MCNPX to Star-CD.

A similar configuration with modified coolant channel geometry is also considered to prevent the beam tube from blocking the returning coolant in the outlet channels. The blockage is caused by the beam tube because it has a slightly larger diameter than those for target disks. In the modified geometry, the target plates are enlarged radially to match the diameter of the beam tube. Although the updated configuration streamlines the flow field and improves the cooling in

the first gap, between the beam window and first target disk, the modification does not reduce the peripheral stresses.

The target assembly configurations with only two inlet channels and two outlet channels, as considered up to this point, result in two symmetric recirculation zones as shown in Fig. 2-15 as an example of typical velocity vectors in the gap between two target disks. Also, the stagnation points near the converging edges of the two inlet and two outlet channels are visible in Fig. 2-15. A careful examination of the calculated thermal stresses reveals that the peak peripheral stresses are related to hotspots. These host spots are associated with the recirculation

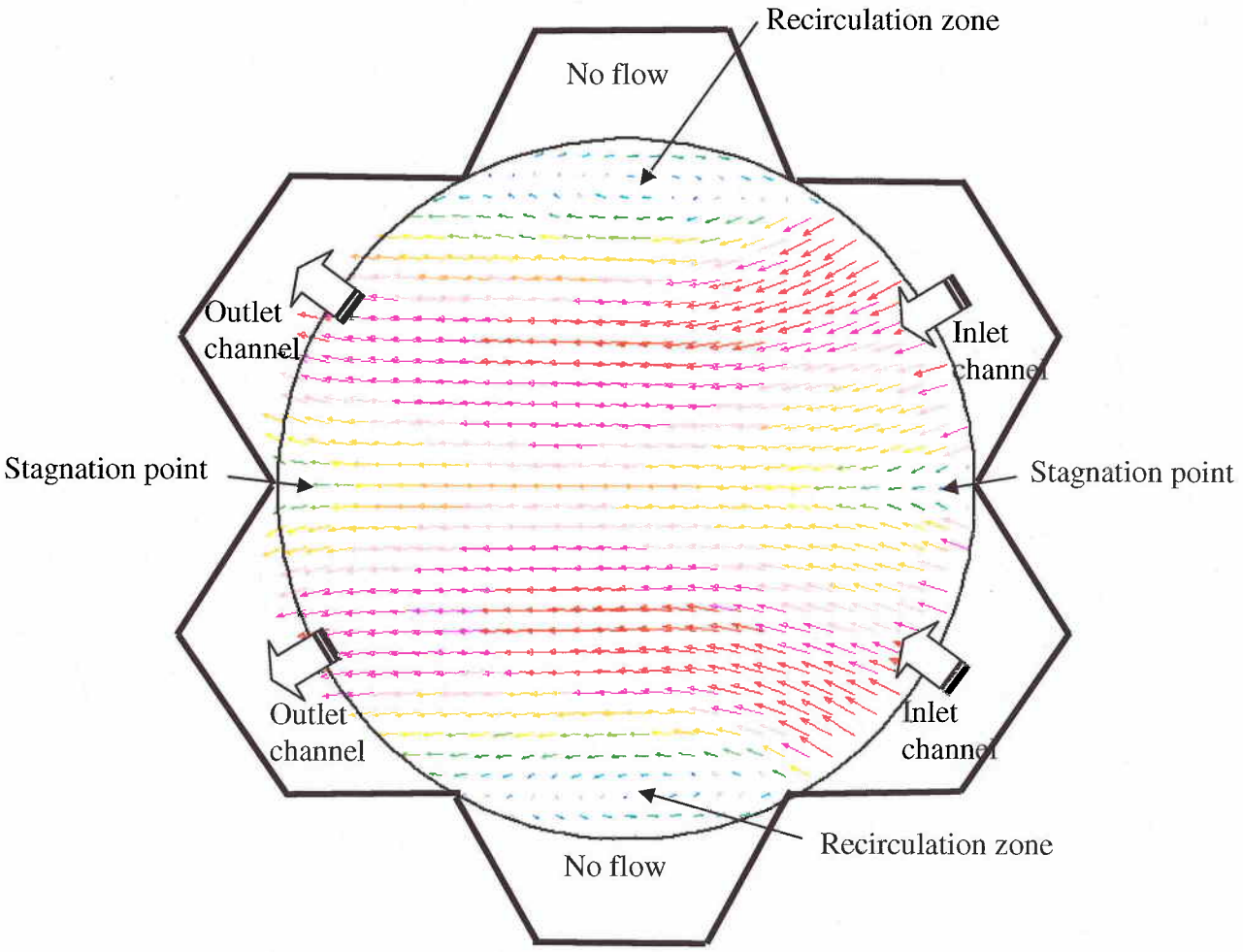

Figure 2-15. Typical velocity vectors in the gap between two target disks for a configuration with two inlet and two outlet coolant channels.

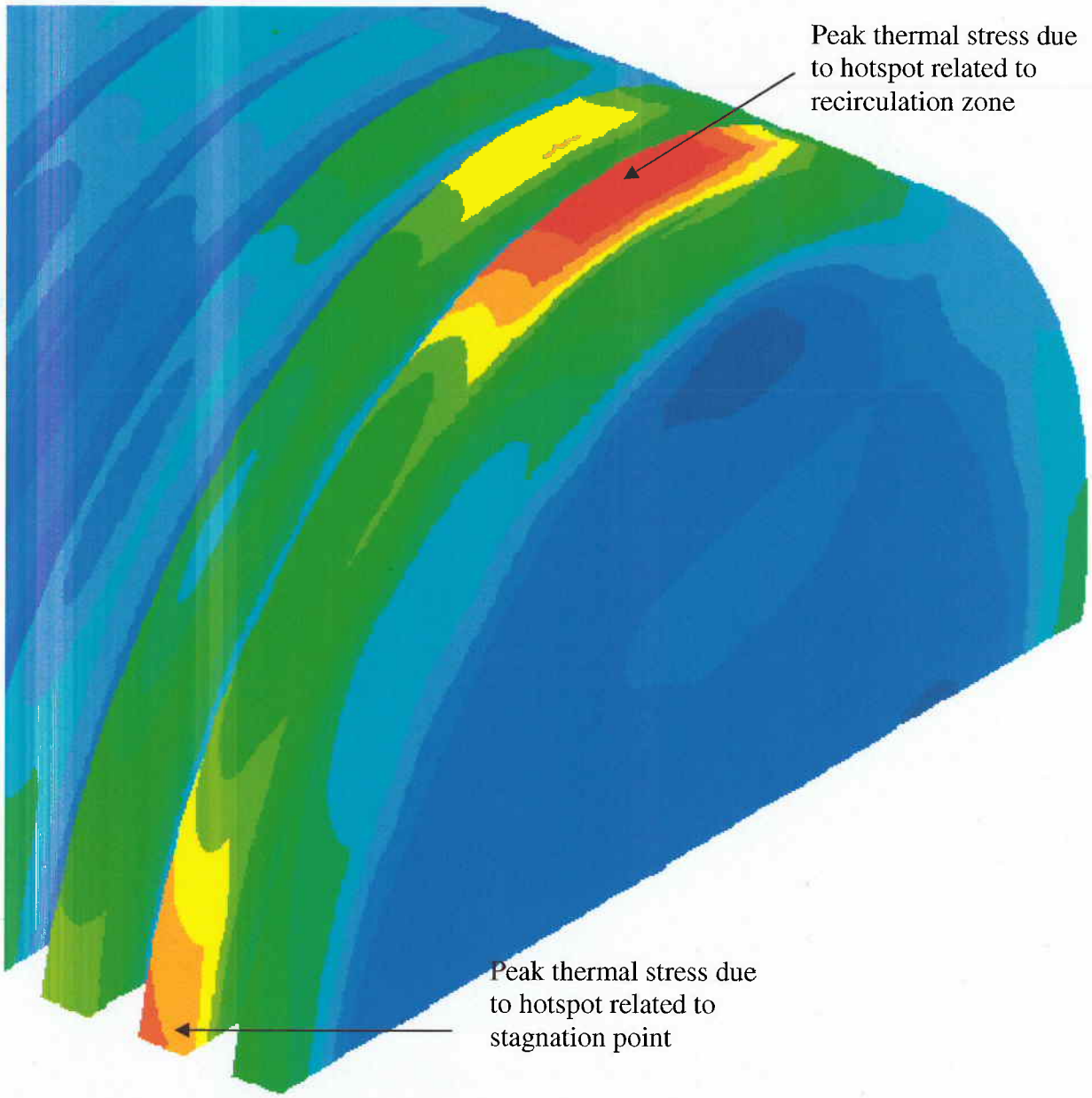

Figure 2-16. Typical peripheral stress contours in uranium target disks for a configuration with two inlet and two outlet channels (for 100 MeV electrons).

zones and their stagnation points as seen in Fig. 2-16 for 100 MeV electrons. The peak stress appears only in one or two target disks, but since the disk thickness cannot be less than about 3 mm for structural considerations, the target assembly design with only two inlet and two outlet channels are concluded to be impractical for the uranium target material.

As a result, a series of three inlet and three outlet coolant channel configurations are evaluated next. In these configurations, the flow rate in the inlet and outlet coolant channels are reduced to maintain the same mass flow rate as of the previous two coolant channel configuration. As expected, when the two idle channels in Fig 2.15 are used, the bottom one as an inlet and the top one as an outlet, the symmetric recirculation zones disappear and the flow field in the gap between the target disks becomes more streamlined. However, the stagnation points near the converging edges of the inlet and outlet channels prevail as seen in Fig. 2-17 as an example. To minimize the impact of the stagnation points on the flow field and thermal stresses, this target assembly concept with three inlet and three outlet channels is further modified by sharpening the converging edges of the inlet and outlet channels as another design change.

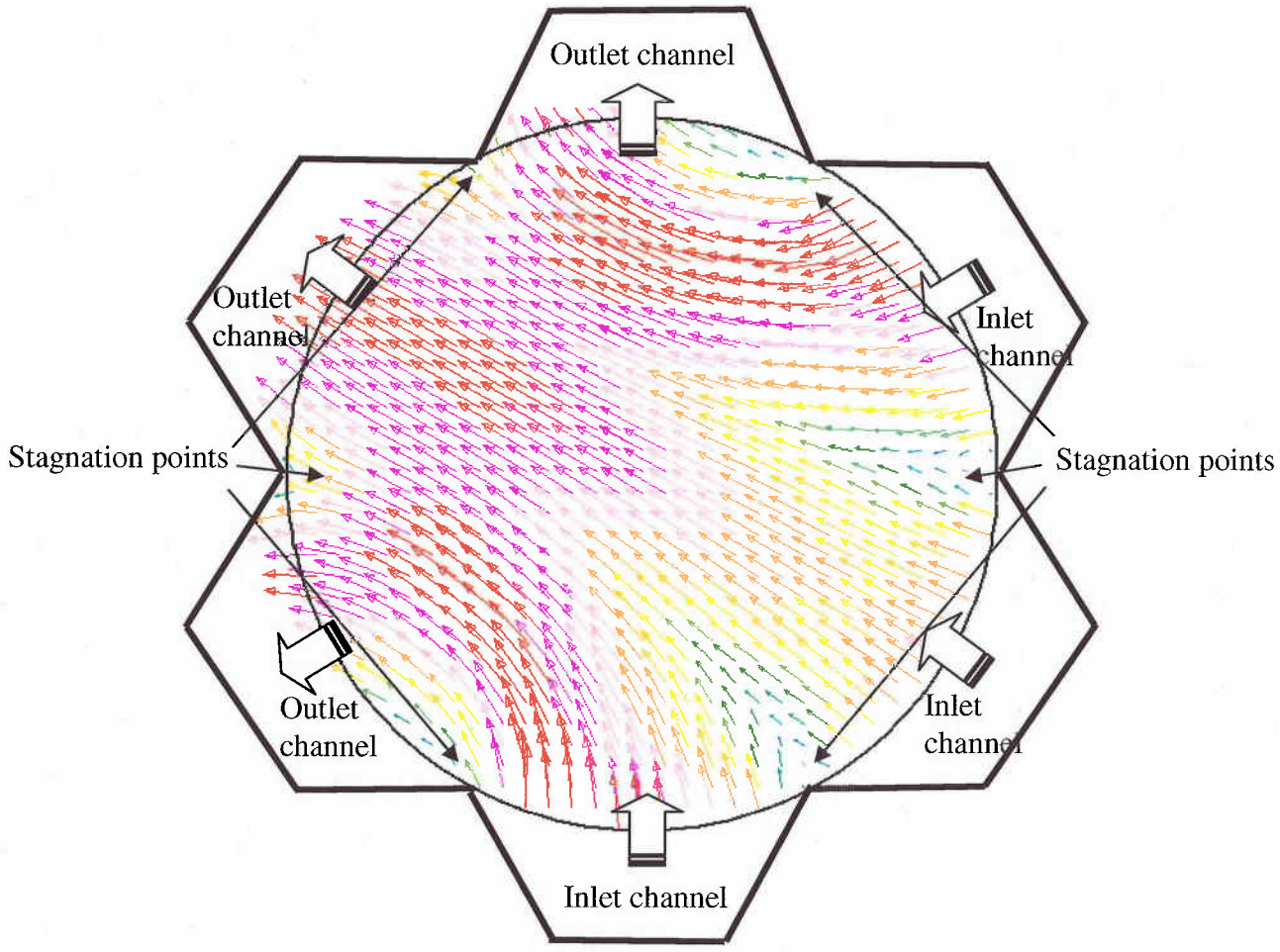

Figure 2-17. Typical velocity vectors in the gap between two target disks for a configuration with three inlet and three outlet coolant channels.

These changes improved the design and resulted in a more uniform thermal stresses distribution along the periphery of the target disks in comparison to the results shown in Fig. 2-16. However, the thermal stresses still high, the peak value is ~390 MPa in the second target disk for the 100 MeV electrons. Since the remaining thermal stresses are associated in part with the temperature gradients in the radial direction, a peripheral gap between the uranium material and the aluminum clad is considered next. The thermal resistance of the gap minimizes the radial temperature gradients and thus the thermal stresses. However, a thin layer of the disk has a peak thermal stress in excess of the target value as shown in Fig. 2-18. The maximum stress is on the surface of the uranium target since the aluminum clad provides a conduction path around the gas gap. To avoid this problem, a zirconium alloy cladding material is also considered but, since it further inhibited axial heat transfer, the calculated target temperatures were prohibitively high for that case.

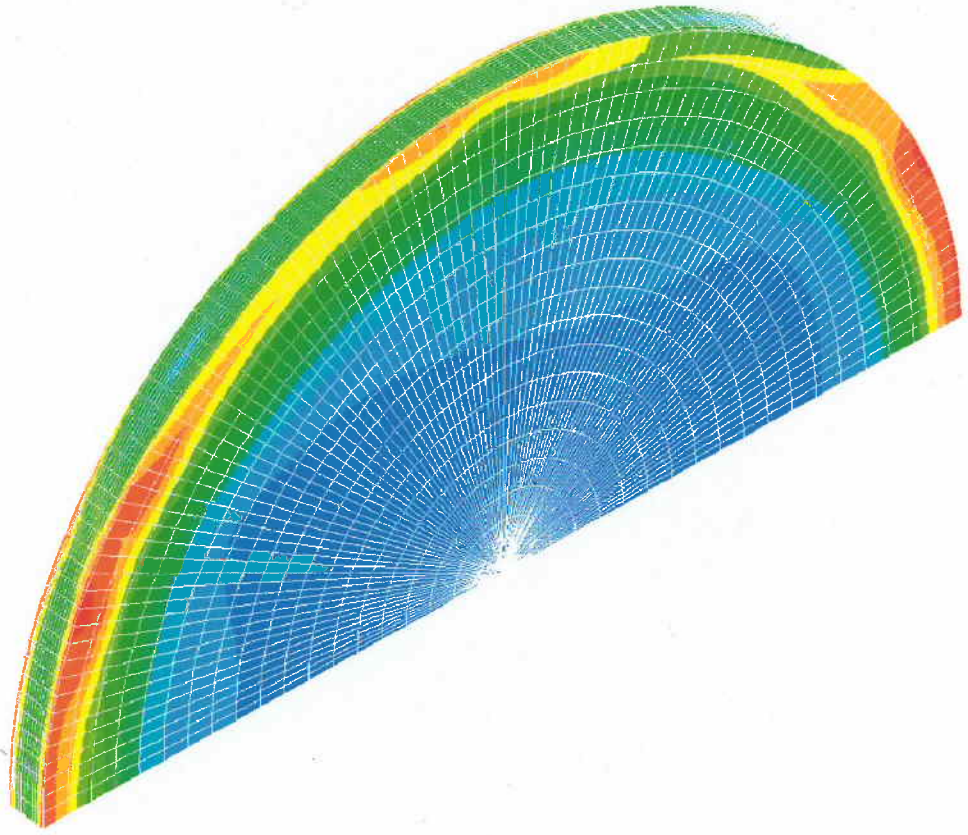

Figure 2-18. Stress contours in the second target disk for a configuration with three inlet and outlet channels and a peripheral gap between uranium and aluminum clad for 200 MeV electrons. The peak stress on surface (shown in red) is 265 MPa.

An identical configuration but with unequal distribution of the flow between the three inlet channels, 40% more flow in the central inlet channel, did not shift the stagnation point away from the sharp corners between the coolant channels. This re-distribution of the flow did not result in reduction in the thermal stresses. Further reducing the thicknesses of the second and third target disks from 3 mm down to 2 mm resulted in a lower temperatures in those disks although the heat load shifted to the fourth and fifth disks further downstream. The peak peripheral stresses in the seconds and third disks were not low enough to provide the needed durability margin.

Another idea was to reduce the diameter of the uranium disks inside the aluminum clad and make it equal to the electron beam diameter. In this configuration, the peripheral thermal stresses remained mostly unaffected. Repeating the analyses with pure uranium-238 disks instead of natural uranium disks did not show any improvements. The pure uranium-238 target is expected to reduce the heat load by eliminating the fission reaction rate of uranium-235 in the target region. However, the neutronics calculations indicated little change in the average heat deposition in the uranium-238 disks in comparison to the natural uranium disks.

Since the reduction in the diameter of the uranium disks produces a small increase in the thermal stresses for natural uranium and pure uranium-238 target materials, a series of calculations using a larger electron beam diameter (7.54 cm) were investigated next. For the 100 kW beam power, the enlarged electron beam diameter implies a reduction in power density (energy deposition per unit volume) in the U disks. A side-by-side comparison of the power density and the temperature distributions is shown in Fig. 2-19 for both small and large beam diameter cases using the partitioning scheme given in Table 2-6. As expected, the lower power density from larger beam diameter case reduces the disk temperatures significantly and improves the thermal stresses. However, the peak peripheral stress in the seconds and third disks still exceeds the 200 MPa design target, which leaves the problem unresolved.

Using the target design with the large beam diameter, two additional flow configurations were analyzed based on altered inlet and outlet channels, as opposed to the configuration shown in Fig. 2-17 with three consecutive inlet and outlet channels on the opposing side of the target

disks. Although such altered inlet outlet configuration avoids the stagnation points at the converging edges of the coolant channels, it creates a larger stagnation point along the symmetry axis of the assembly. This flow configuration creates a substantially larger hotspot where the heat deposition has a maximum value. Consequently, the peak stresses are about 60% larger in this case. To avoid this hotspot at the center, a nonuniform flow between the altering inlet channels were also evaluated but it did not lead to improved conditions.

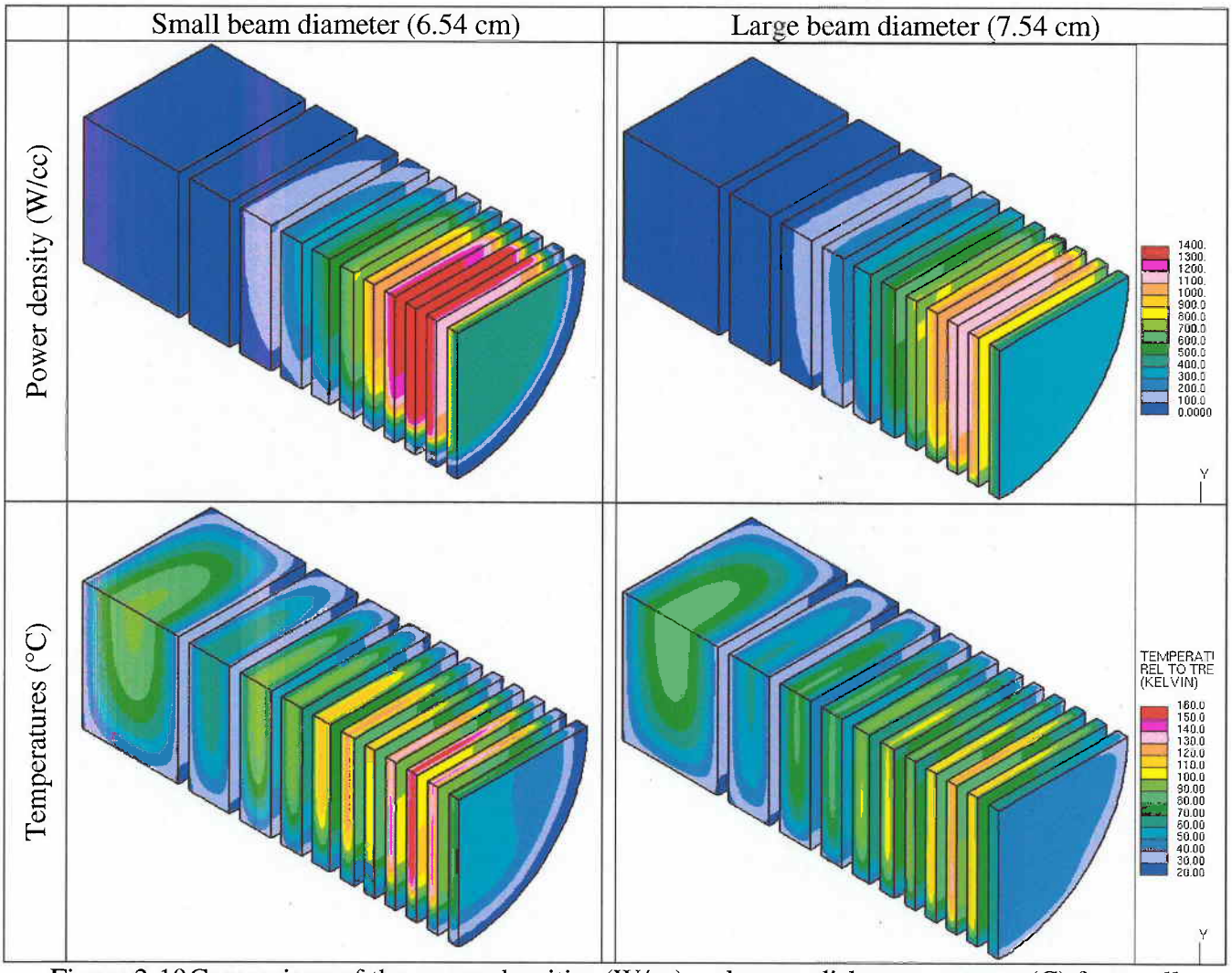

Figure 2-19Comparison of the power densities (W/cc) and target disk temperatures (C) for small and large beam diameters with 200 MeV electrons.

An obvious extension of the last configuration with the large beam diameter was to include a thin peripheral gap between the uranium material and the aluminum clad to provide thermal insulation for reducing the radial temperature gradients. This extension indeed improved the target design, reducing the peak stress in the third disk by 15% down for the 200 MeV electrons to satisfy the design target. Therefore it is accepted as the final configuration for Al-clad uranium target assemblies for the electron beam with circular cross-section.

Another practical approach to implement the thermal insulation is to use a radial "rut" (an indentation in the Al clad outer surface), which is also analyzed. Although it resulted in a slightly higher peak thermal stress, 212 MPa in the third disk for 200 MeV electrons, this configuration is considered as a viable alternative due to ease of manufacturability. Since the peak thermal stresses appear around the stagnation points, another case in which a thermally insulating layer is considered only near the converging edges of the coolant channels is evaluated as well; however, it produced much higher thermal stresses.

3. Results for Square Electron Beam Profile and Target Disks

Based on the updated design of the electron beam transfer channel, the second phase of the target studies focused on a uniform electron beam with a square cross section. A cutaway of exploded view of the target assembly for the square target plate configurations is shown in Fig. 3-1. The heat deposition distributions for the square beam cases were obtained using full three-dimensional MCNPX models. Since tungsten targets proved to be fairly benign in terms of temperature and thermal stresses limits, only square-plate uranium target configurations were studied.

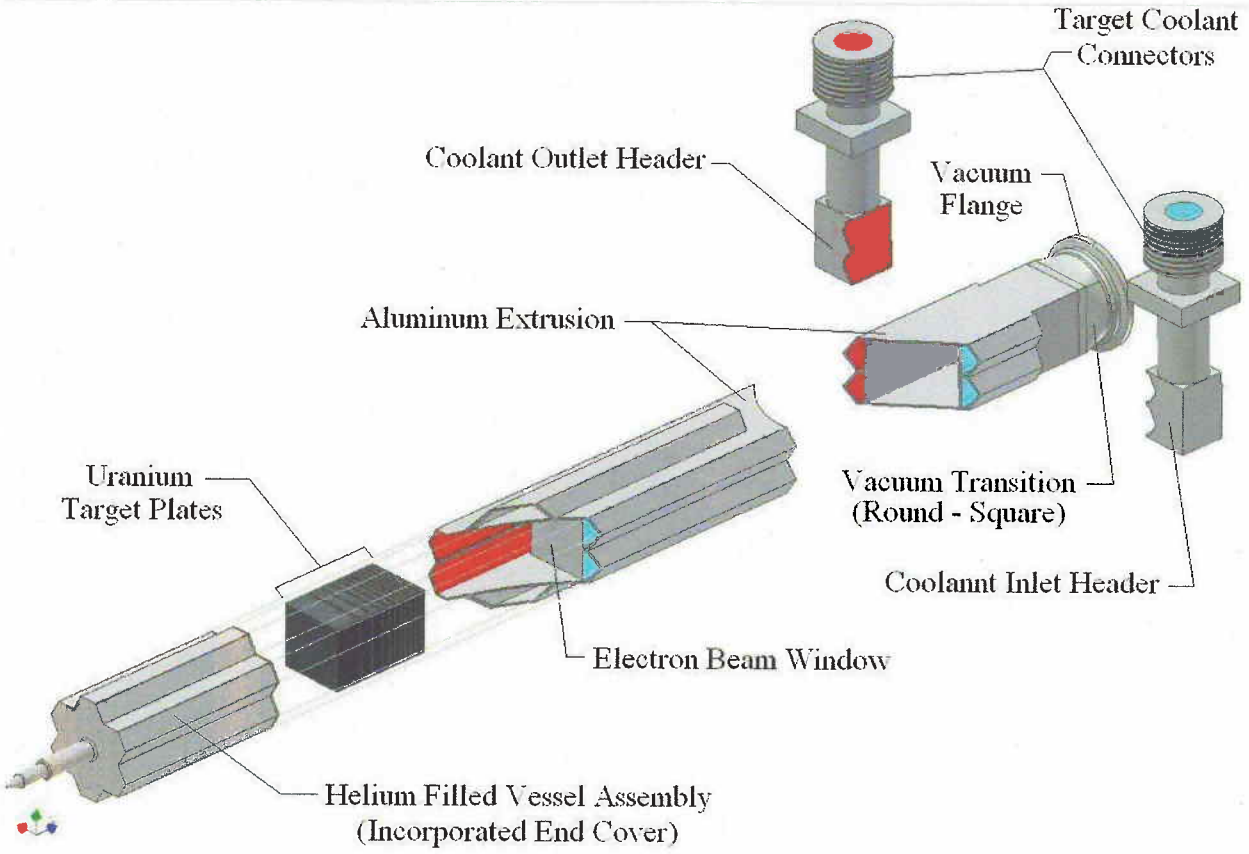

Figure 3-1. Exploded target assembly cutaway for an electron beam with square cross section.

3-1. Al-Clad Uranium Targets

Taking advantage of the gained experience from the previous target disk studies for circular electron beam profile, the first configuration considered has the 11 square-plates and the partitioning scheme shown in Table 3.1. The dimensions of the target for this configuration are

64.6x64.6 mm^2 excluding peripheral aluminum clad. Only two inlet and two outlet channels are used. Taking advantage of the symmetry in the problem, only the upper half of the target assembly is modeled. This configuration is analyzed with coarse and fine grid models. The results of the coarse-grid model with 744,000 computational cells are found to be fairly consistent with those of the fine grid model shown in Fig. 3-2 with 2.64 million computational cells (916,000 in the fluid zone). Therefore, grid independent solutions are obtained with both models.

Table 3-1 Partitioning scheme for eleven square-plate uranium target.

Coolant channel #	Gap thickness (mm)
1	1.
2	1.75
3	1.75
4	1.75
5	1.75
6	1.75
7	1.75
8	1.75
9	1.75
10	1.75
11	1.75
12	1.
Total	19.5

Disk #	Target disk thickness (mm)
1	3.0
2	3.0
3	3.0
4	3.0
5	3.0
6	4.0
7	5.0
8	6.0
9	9.0
10	12.0
11	28.0
Total	79.0

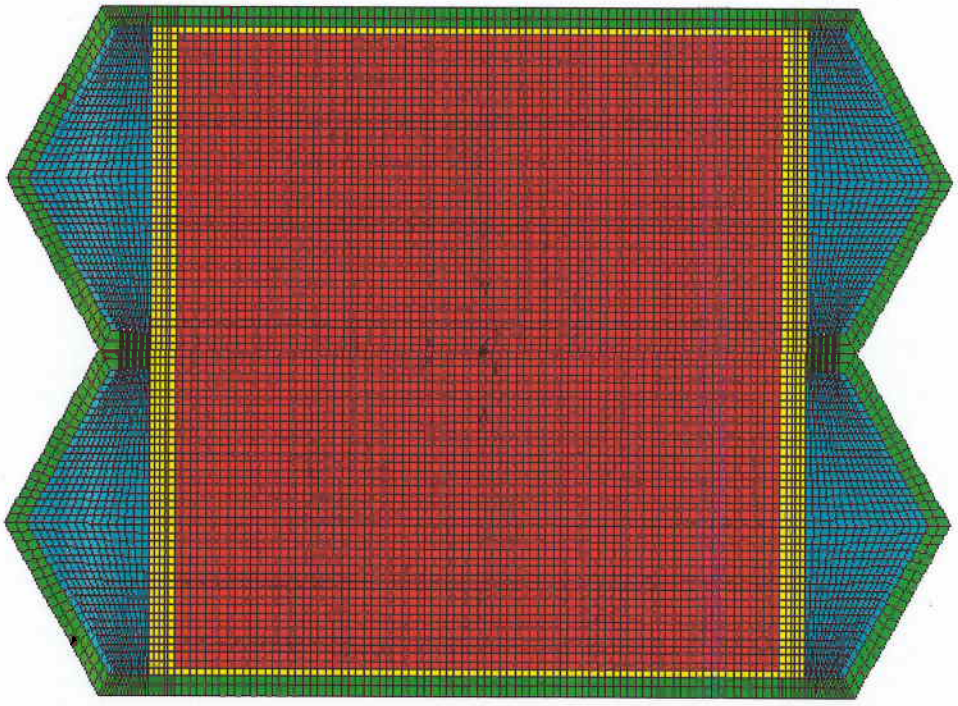

Figure 3-2 Refined-grid for a square target-plate configuration. The red colored zone is for the uranium target, yellow for the aluminum clad, green for the structural frame, and blue for the water coolant.

The power density distributions obtained with the three dimensional MCNPX models are shown in Fig. 3-3, and the corresponding target plate temperature distributions are shown in Fig. 3-4 for both the 100 and 200 MeV electrons. The maximum target plate temperatures are calculated as 243.4°C and 248°C for 100 MeV electrons, and as 203°C and 206°C for 200 MeV electrons with the coarse and fine grid models, respectively. Although the differences in calculated temperatures and flow field are fairly small for the CFD solver, the coarse and fine grid solutions make a notable difference for the stress calculations. The estimated peak thermal stresses are 415 and 460 MPa based on the CFD solutions with the coarse and fine grid models, respectively. Therefore, to be on the conservative side, the rest of the configurations studied are based on the fine grid solutions.

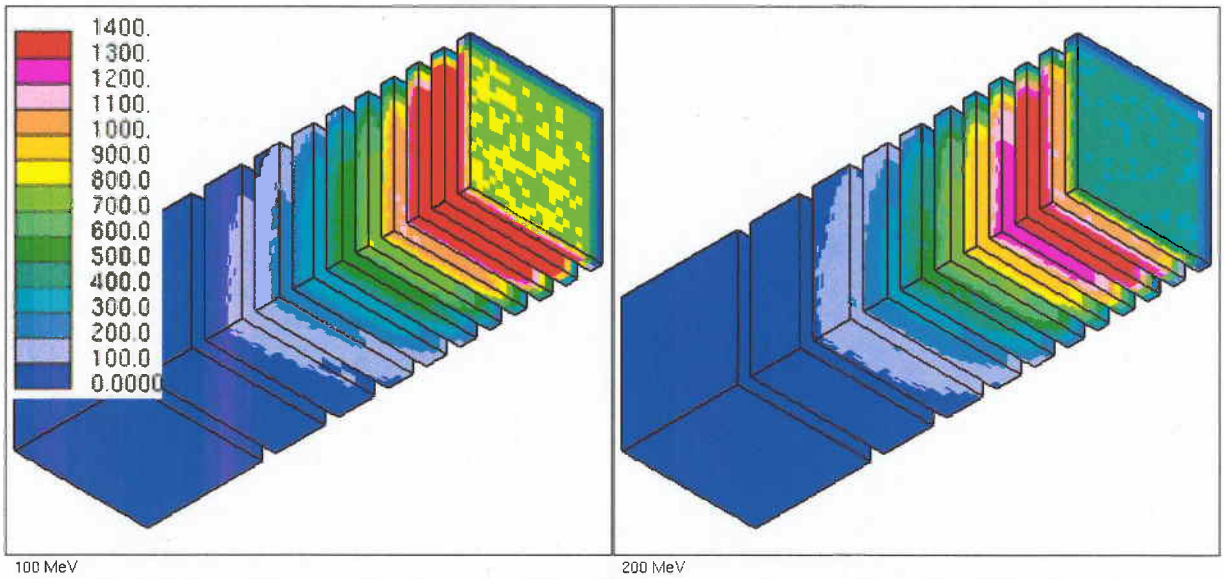

Figure 3-3. Power density distributions (W/cm^3) in square target-plates for 100 MeV electrons (left) and 200 MeV electrons (right)

Initially 7 m/s nominal flow velocity is assumed at the inlet channels. Due to parallel orientation of the inlet and outlet channels with this square-plate configuration, the flow field between the target plates is much more streamlined with no recirculation zones as seen in Fig. 3-5. However, the ribs that extend along the beam tube separating the two inlet and two outlet channels still create two stagnation points (one on the inlet side, and another on the outlet side), leaving a relatively low flow zone in the middle. To avoid this strip with low flow, the ribs are removed from the design and the same configuration was analyzed for the same flow rate.

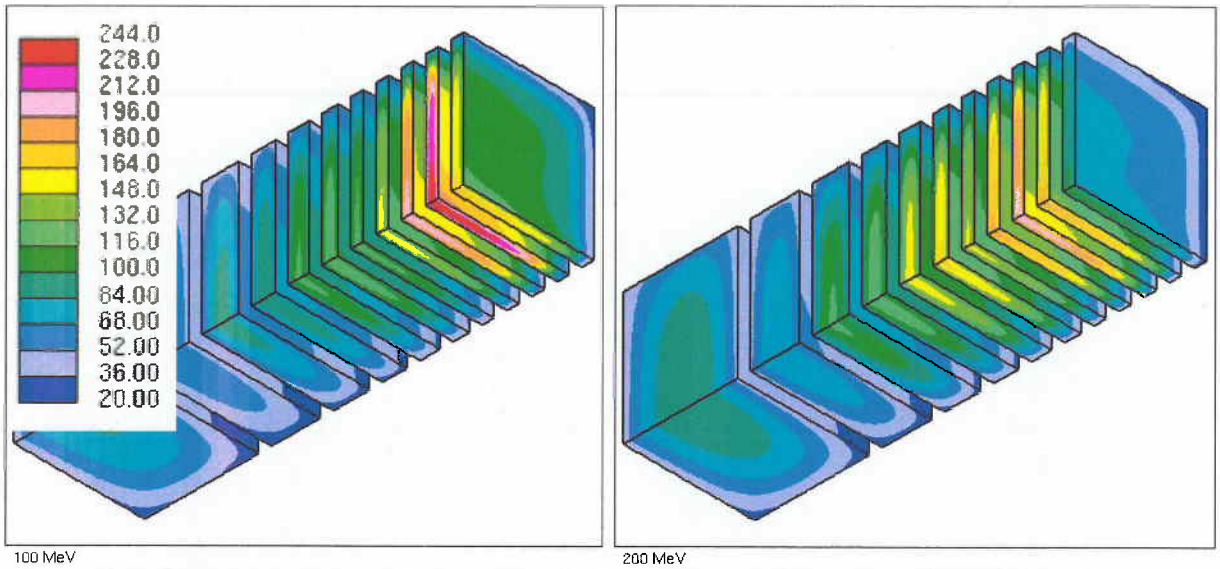

Figure 3-4 Temperature distributions (°C) in square target-plates for 100 MeV electrons (left) and 200 MeV electrons (right).

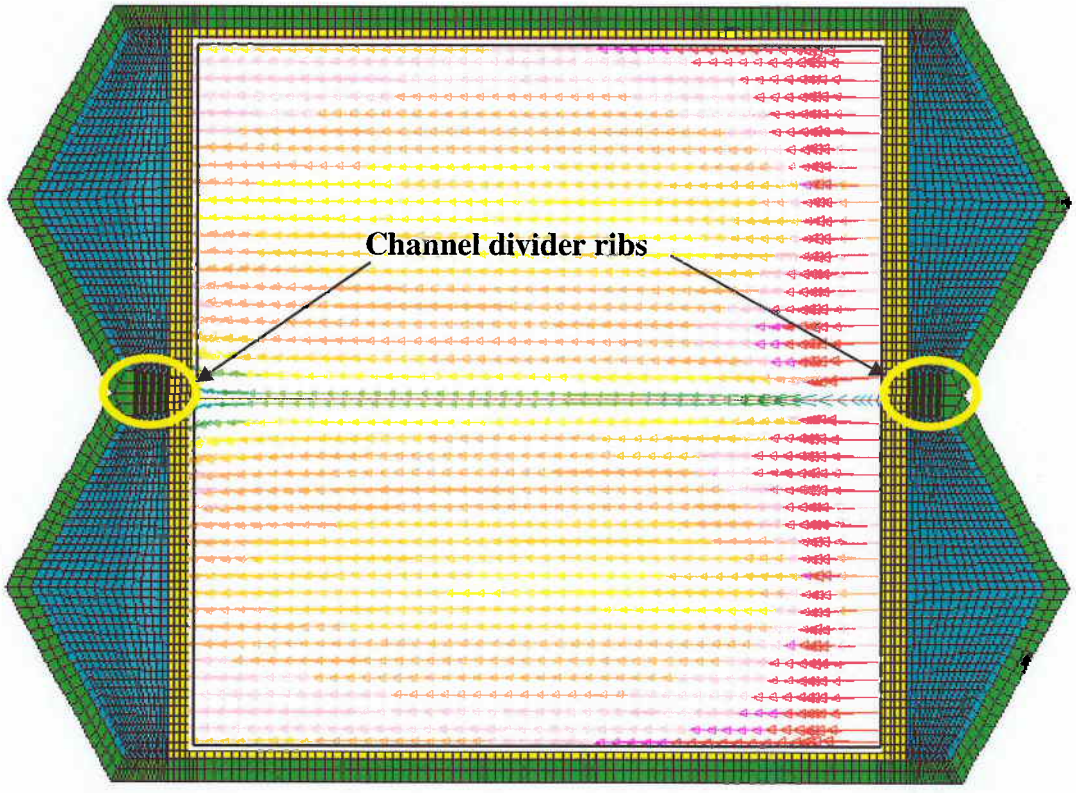

Figure 3-5. Typical flow field (velocity vectors) in the middle of the 1.75 mm narrow gap between the target plates. The strip with low flow is due to the ribs that separate the two inlet and two outlet coolant channels.

As expected, removing the ribs eliminates the strip with lower velocities and reduces the predicted peak plate temperature significantly, by 24°C for 100 MeV electrons and 12°C for 200 MeV electrons. That has even a larger impact on the resulting thermal stresses, reducing the peak stress in the third plate at the contact point of the ribs and the plates by 15% for 200 MeV electrons. Nevertheless, the predicted thermal stresses are still significantly higher than the target value of 200 MPa.

Increasing the nominal flow rate in the inlet channels from 7 m/s to 10 m/s results in further reductions in peak plate temperature (down by 33°C to 191°C for 100 MeV electrons, and down by 29°C to 164°C for 200 MeV electrons) and peak thermal stress (down by 60 MPa to 334 MPa in the third plate for 200 MeV electrons). The calculated stresses have a somewhat similar pattern for the square target plates as for the circular target disks with peak values along the periphery. But unlike the circular target disks where the stresses are fairly uniform along the periphery, the stresses are minimal at the sharp corners of the square plates and they peak along four edges as shown in Fig. 3-6. This stress pattern is generally due to non-uniform temperature distribution between the center and the periphery. The disk center needs to expand radially because of its higher temperatures but it is constrained along the edges with the lower temperatures.

To reduce the peak thermal stress, a series of other configurations were considered. In the first configuration, a reduced U target surface area with 60×60 mm^2 cross section (excluding the peripheral Al clad) is evaluated with 7 m/s coolant velocity in each coolant channel. This configuration results in only 12% reduction in peak stress in the third target plate for 200 MeV electrons. When a peripheral gap between the U meat and Al-clad is included in this configuration with the reduced U surface area, another 11% reduction is achieved, bringing the peak stress down to 308MPa in the third plate for 200 MeV electrons. A drastically radical concept with turbulence inducing ribs in the narrow gaps between target plates reduces mildly the plate temperatures and does not translate to lower thermal stresses.

In another configuration, instead of a reduced U target surface area, larger electron beam cross-section area is considered. In this case, the electron beam is assumed to have a 64×64 mm^2

cross section area while the uranium target area is retained as 64.6×64.6 mm^2. Due to the enlarged beam profile, this configuration results in a reduced power density, and therefore, about 19°C lower peak plate temperature as shown in Fig. 3.7. The lower power density and core temperatures also translate to about 20% reduction in the peak stress (~80 MPa). When a peripheral gap between the U meat and Al-clad is added to this configuration with low power density, another 15% reduction in the peak thermal stress is achieved, bringing down the value for the third plate to 268 MPa for 200 MeV electrons. Although this peak stress is still higher than the 200 MPa design target, the enlarged beam profile (lower power density) clearly provides better results with lower target plate temperatures and thermally induced stresses. As a result, an enlarged beam profile (with a 64×64 mm^2 cross section area) has been considered consistently in the remaining case analyses.

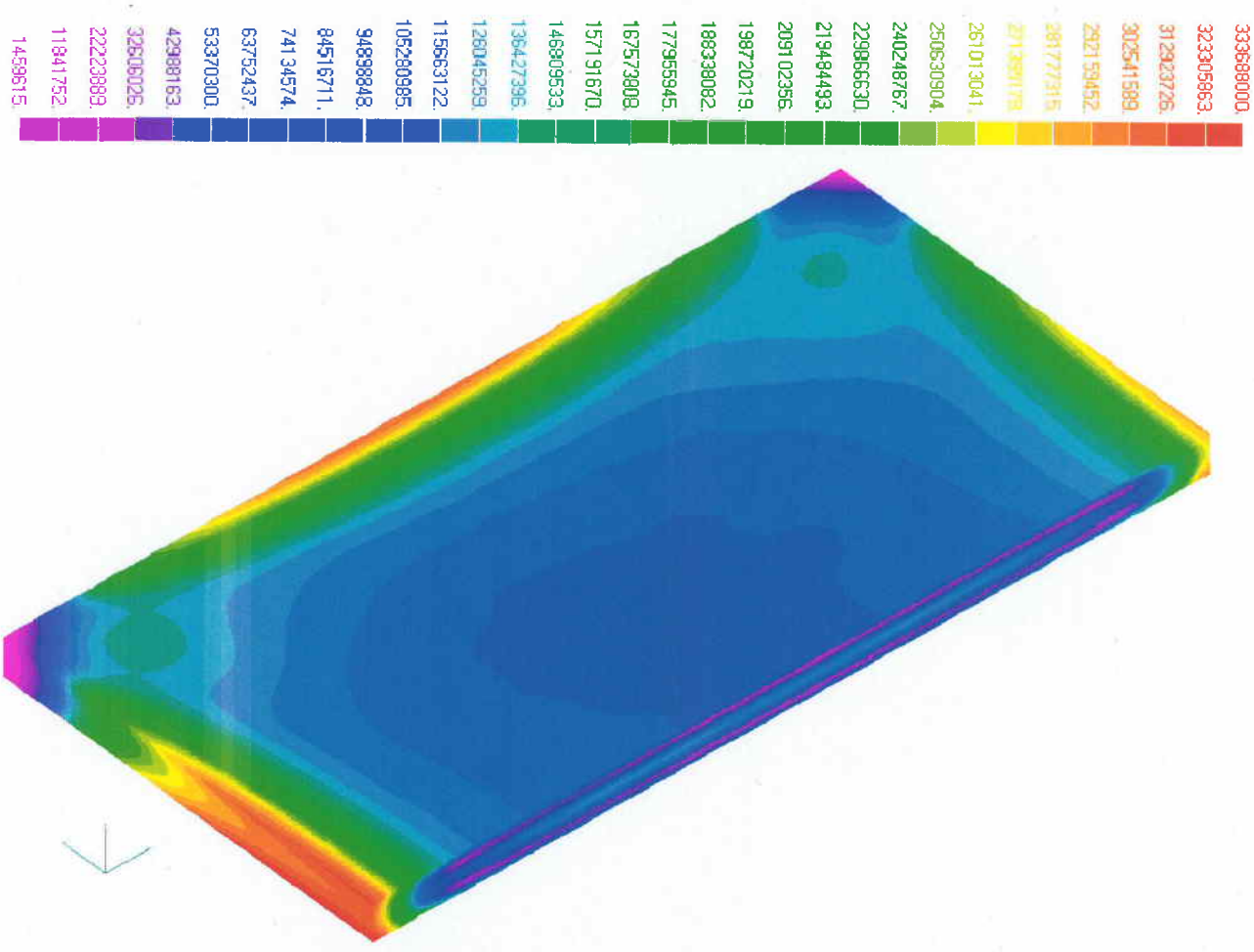

Figure 3-6. Typical stress distributions in the square uranium target plates.

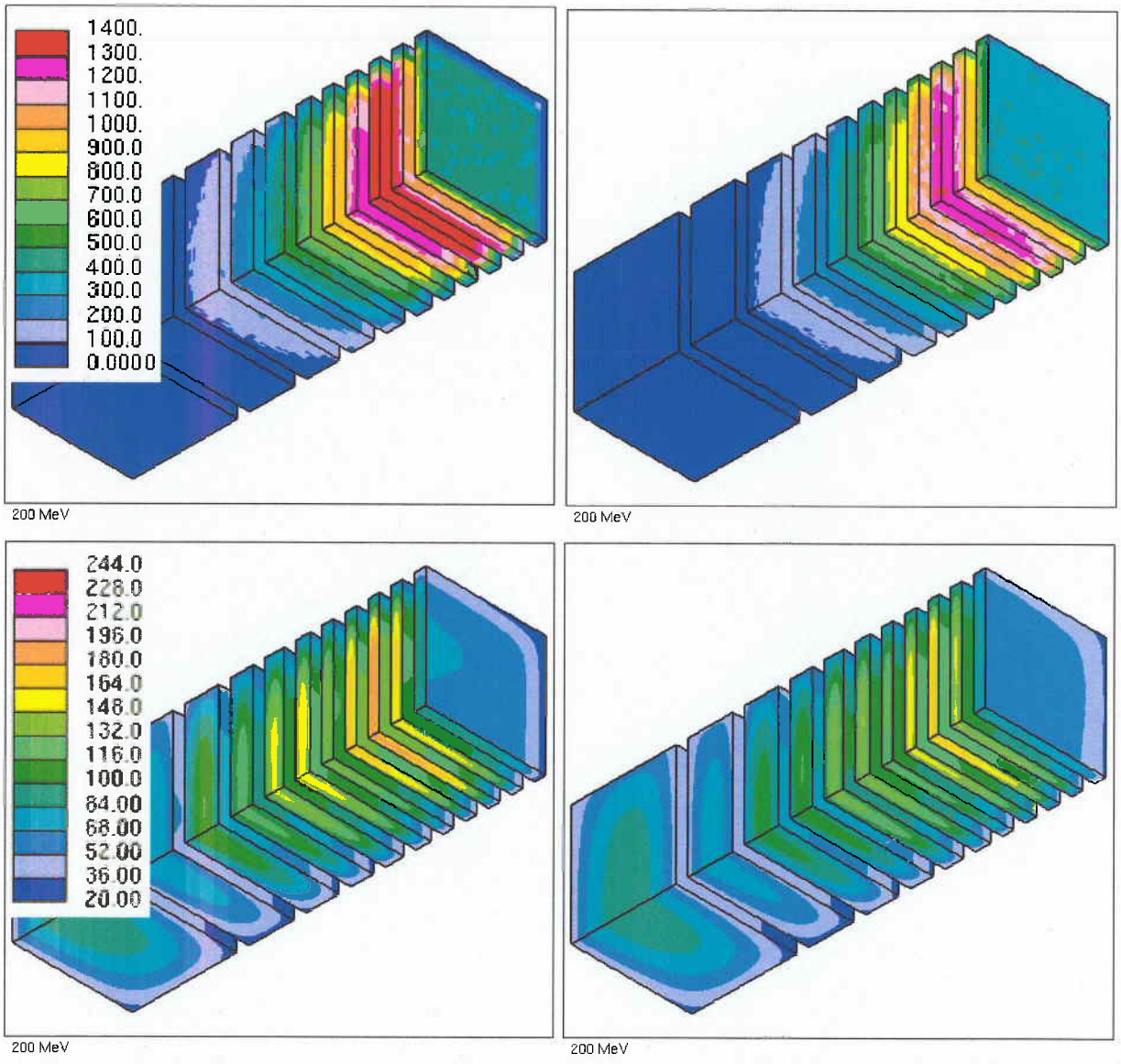

Figure 3-7 Power density distributions (in W/cm^3) in top row, and the corresponding temperature distributions (in °C) in bottom row with 60×60 mm^2 beam profile (left column) and 64×64 mm^2 beam profile (right column). All plots are for 200 MeV electrons.

The results from the earlier configurations consistently predict the peak temperatures and stresses in the second target plate for 100 MeV electrons, and in the third target plate for 200 MeV electrons. Therefore, one obvious solution is to further reduce the thickness of U target material in these plates. For the smaller heat load with thinner target material, the temperatures and thermally induced stresses are also expected to decrease in proportion to the thickness reduction. A configuration with reduced thickness (2.5 mm) for the first five target plates is

considered next. To compensate for the reduction in the uranium thickness, the thicknesses of the aluminum clad on both sides of these thin plates are increased from 0.7 mm to 0.95 mm to maintain the structural integrity of the thin plates. The target plate temperatures for this new configuration are compared to the results for the earlier configuration in Fig. 3-8.

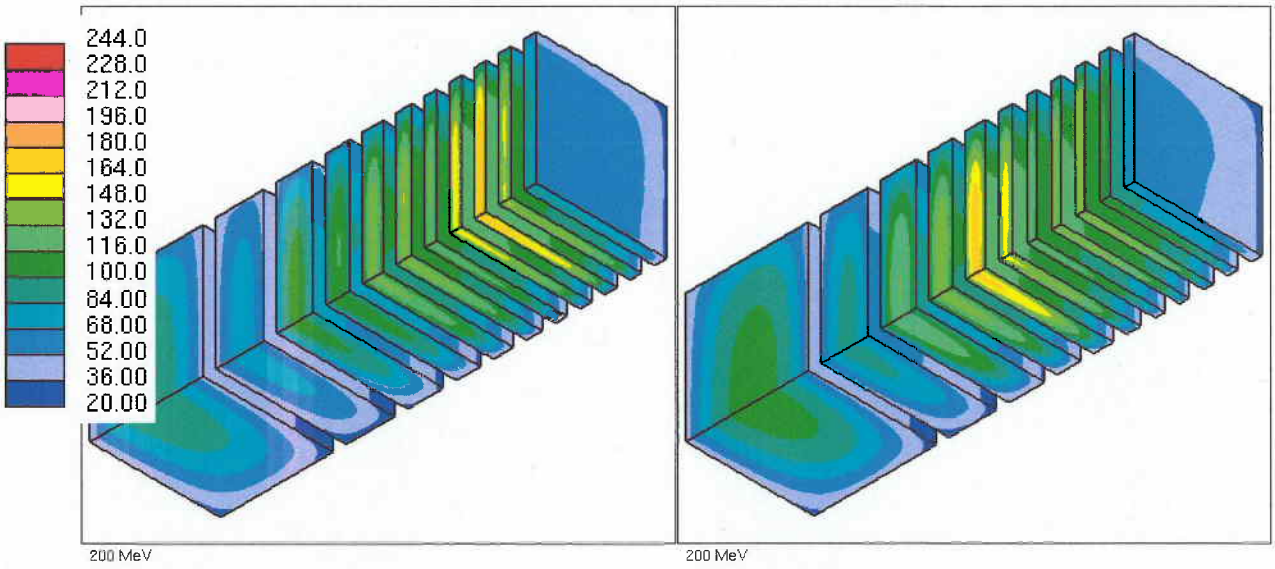

Figure 3-8 Temperature distributions (in °C). Left plot is for the first configuration with 3 mm uranium thickness in first five target plates, and the plot on right is for the second configuration with 2.5 mm uranium thickness in first five plates. The results are for 200 MeV electrons and 64×64 mm^2 beam profile.

Although the peak temperature remains more or less the same (172°C), location of the peak shifts from the third plate to seventh plate in the new configuration, effectively reducing the peak stress in the third plate by 21% down to 248 MPa for 200 MeV electrons. The same configuration but with 10 m/s nominal flow rate instead of 7 m/s in the inlet channels reduces the peak temperature by 14% (again, in the seven plate) and peak stress in the third plate by an additional 15% (down to 211 MPa) for 200 MeV electrons. Finally, including a peripheral gap between the U material and Al-clad brings the peak stress down to 180 MPa in the third plate for 200 MeV electrons. For 100 MeV electrons, the peak stress is estimated as an acceptable value of 206 MPa in the first six plate of this configuration.

To address the undesired peak stress in the seventh plate, the 11-plate partitioning scheme is further evaluated with readjusted thicknesses for the last four plates. Such readjustment does not alter the estimated peak temperatures; however, it redistributes the heat load for a more balanced temperature distribution between the plates. Still, the heat load in the last 32 mm thick plate results in a significantly high peak thermal stress; about 256 MPa for 100 MeV electrons, and 290 MPa for 200 MeV electrons. Eliminating the peripheral gap between the U material and Al cladding for the last three thickest plates help reduce the core temperatures and the peak stress in the last plate down to 230 MPa

Consequently, a final 12-plate partitioning scheme is considered for aluminum clad uranium target design with square cross section. Two separate configurations with different plate thicknesses are studied for this partitioning scheme, the last configuration successfully satisfying all the neutronic, thermal, and structural design criteria. The plate and coolant gap thicknesses for this final configuration are given in Table 3-2. Again, the thickness of the aluminum clad is 0.95 mm on both sides of 2.5 mm thick plates, and 0.7 mm for other plates. This configuration has 64.6×64.6 mm^2 surface for U target for 64×64 mm^2 electron beam cross sectional area. It also includes a peripheral gap between the uranium material and aluminum clad for all but the last four target plates. For a nominal 10 m/s flow rate in two inlet channels, the power density and corresponding temperature distributions are shown in Fig. 3-9.

Table 3-2 Partitioning scheme for twelve square-plate uranium target.

Coolant channel #	Gap thickness (mm)
1	1.
2	1.75
3	1.75
4	1.75
5	1.75
6	1.75
7	1.75
8	1.75
9	1.75
10	1.75
11	1.75
12	1.75
13	1.
Total	21.25

Disk #	Target disk thickness (mm)
1	3.0
2	2.5
3	2.5
4	2.5
5	3.0
6	3.0
7	4.0
8	5.0
9	7.0
10	10.0
11	14.0
12	22.5
Total	79.0

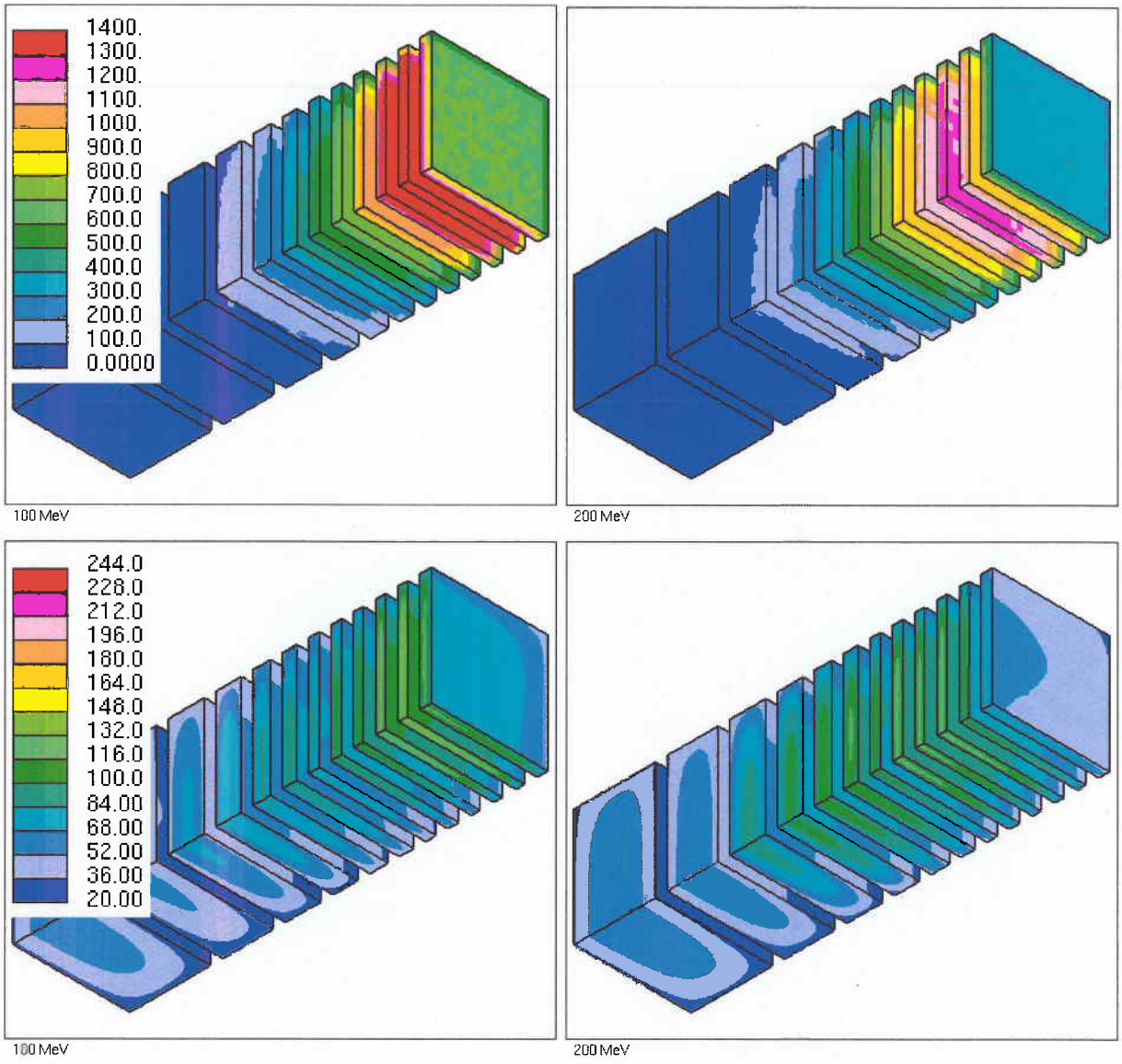

Figure 3-9. Power density distributions (W/cm^3) in top row, and the corresponding temperature distributions (°C) in bottom row for the final square-plate U target configuration with 100 MeV electrons (left column) and 200 MeV electrons (right column).

In the final square-plate target configuration, the peak temperature is predicted as 144 C for 100 MeV electrons in the second plate, and 127 C for 200 MeV electrons in the third through the fifth plate. The stresses in the first seven plates of the assembly are also shown in Fig. 3-10. The stresses in the remaining last five target plates are substantially lower than in the first seven. Although the peak stress is slightly higher than the 200 MPa design target for 100 MeV electrons, this final square-plate U target configuration provides sufficiently comfortable structural margin

for sustained operation, especially considering that calculated thermally induced stresses are secondary stresses in nature.

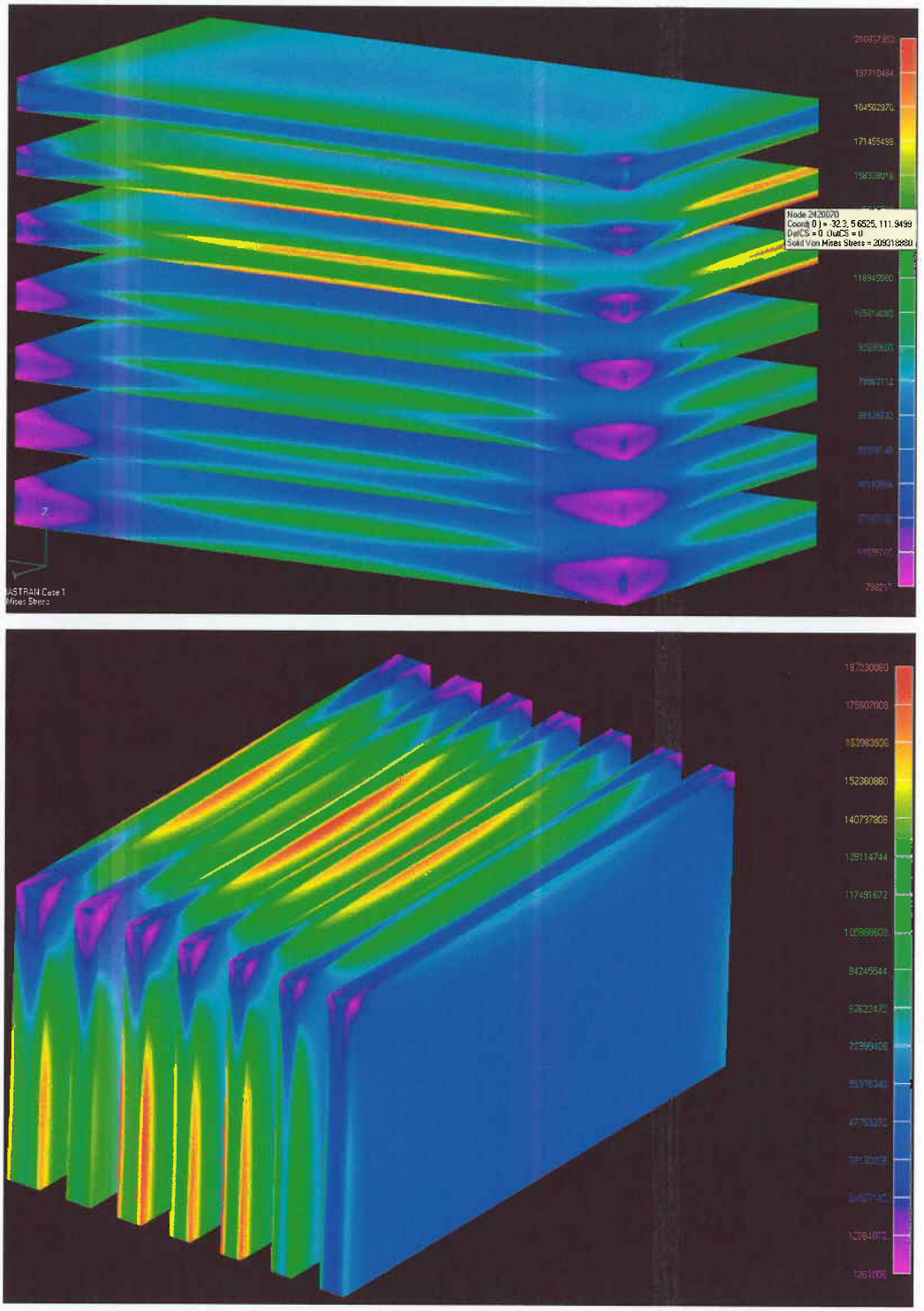

Figure 3-10. Thermal stresses (Pa) for the final square-plate U target configuration with 100 MeV electrons (top) and 200 MeV electrons (bottom).

Summary and Conclusions

As a part of the conceptual design development of an accelerator-driven subcritical facility, the high-fidelity analyses of various target options have been performed with formulations reflecting the three-dimensional geometrical details of each concept. Tungsten and uranium are considered as the target materials for generating neutrons from electron interactions. The electron beam has a uniform spatial distribution and circular or square cross-section. The optimization of the target assembly configurations is performed via sequential neutronic, thermal-hydraulic, and structural analyses for a comprehensive assessment of multi-physics phenomena affecting each design concept. In addition to geometric modifications to streamline the flow field and avoid hotspots, the target analyses included evaluation of inlet/outlet configurations, target plate and coolant channel partitioning, flow rate manipulations, beam profile variations, and cladding material alternatives.

The facility is configured for a 100 kW electron beam power to drive the subcritical assembly that consists of an array of hexagonal fuel elements consisting of low-enriched uranium oxide in aluminum matrix. The electron beam interactions with the target material and the neutronic response of the subcritical assembly are evaluated using the MCNPX code to characterize the spatial energy deposition in the target assembly. The Star-CD CFD software is used for the thermal-hydraulic analyses to evaluate the impact of recirculation and stagnation zones and resulting hotspots. The structural analyses are performed mostly with NASTRAN using the temperatures calculated with CFD model. The optimizations are pursued for maximizing the neutron yield, streamlining the flow field to avoid hotspots, and minimizing the thermal stresses to increase the durability.

For the scoping calculations, initially an axially-varying power density distribution is considered only in the target material. The more detailed assessments are based on axisymmetric models with r,z-dependent power density profile for the electron beam with circular cross section, and full three-dimensional models with x,y,z-dependent power density profile for the electron beam with square cross section. Both tungsten and uranium target materials are considered for

100 and 200 MeV electrons. The heat deposition spatial profiles require the use of thin target plates next to the beam window to satisfy the engineering design requirements.

Various target plate and coolant channel thickness are evaluated and optimal neutron yield is achieved with 1.75 mm narrow coolant channels between target plates. Although the neutron spectra from tungsten and uranium are similar, which allows the use of either material in the subcritical assembly without changing its characteristics, the higher neutron yield from uranium target is found to increase the neutron flux in the subcritical assembly. Therefore, a greater emphasis is placed on the optimization of the uranium target. The uranium plates are considered to be covered with 0.7-0.95 mm thick Aluminum-alloy cladding to avoid coolant contamination with fission products.

The thermal-hydraulic analysis of each target design is performed with three-dimensional CFD solutions to verify the compliance with the thermal design criteria. The main design constrain is to maintain the water temperature 50°C below the boiling point, 150°C at 4 atm. Due to the high speed flow (7 to 12 m/s average velocity), a fully developed turbulent flow is established in the inlet and outlet coolant channels of the target assembly. However, the turbulence in the flow field quickly dissipates in the narrow gaps between the target plates resulting in a laminar heat transfer for cooling the target plates. In all configurations studied, the temperature difference between the inlet and outlet coolant is less than 5°C. However, the poor heat transfer in the laminar regime results in significantly higher target plate temperatures.

With uniform 1.75 mm thick gap between the target plates, the distribution of flow between each channel is substantially different, highest flow rate being closest to the beam tube. This unevenness of the flow rate in the gaps between the target plates helps improve the thermal-hydraulic design since it results in better cooling for the first set of target disks that are exposed to much higher heat loads. Still, the recirculation and stagnation zones predicted with CFD model, especially with circular target disks, result in substantial local variations in temperatures. Therefore, the major thermal-hydraulic design challenge has been to streamline the flow field to avoid hotspots. This has been less of a concern with square target plates.

The calculated temperatures are subsequently used for the structural analysis of each target configuration to satisfy a set of engineering design requirements. The main structural performance criterion is to keep peak thermal stresses well below the yield point of the corresponding material, ~200 MPa for uranium target. Due to its high thermal conductivity, temperatures and thermal stresses in tungsten target disks are significantly lower than uranium target disks. In order to keep the thermal stress below the design target, the aluminum-clad uranium target plates have to be cooled more aggressively with 70% more flow rate relative to the tungsten target.

Although a significant thermal gradient exists in thin target plates along the beam direction, the limiting thermal stresses are generally observed peripherally around the edge of target disks/plates. Also, the deformations of the target disks are found to be insignificant, eliminating the concerns for blockages in narrow coolant channels. In order to limit the stresses, the uranium-target assembly design for the electron beam with circular cross section has to be cooled through three inlet and three outlet channels with 12 m/s average coolant velocity. The uranium-target assembly design for the electron beam with square cross section requires only two inlet and two outlet channels with 10 m/s average coolant velocity.

Additionally, to reduce the peripheral thermal stresses in the target plates, a thin insulating gap along the edge of uranium target material and surrounding aluminum clad is included in the design for both circular disks and square uranium-target plates. This insulating gap is found to reduce the temperature difference between the plate center and near the edges, reducing the thermal gradients. The gap is also utilized to collect the gaseous fission products, reducing the swelling.

At the end, keeping the thermal stress below the design target, the thickness of the first set of plates had to be limited to only 3 mm for tungsten and 2.5 mm for uranium target. For those 2.5 mm thin U target plates, thickness of the aluminum clad is 0.95 mm on each side to provide additional structural support.

References

1. "Accelerator-Driven Sub-critical Assembly: Concept Development and Analyses," Y. Gohar, et.al., The RERTR-2004 International Meeting on Reduced Enrichment for Research and Test Reactors, Vienna, Austria, November 7-12, 2004.
2. "Accelerator Driven Subcritical Facility Design Concept," Y. Gohar, I. Bolshinsky, H. Belch, D. Naberezhnev, T. Sofu, A. Talamo, Z. Zhong, Eighth International Topical Meeting on Nuclear Applications and Utilization of Accelerators (AccApp'07), Pocatello, Idaho, July 30-August 2, 2007.
3. "Design and Analysis of KIPT Electron Accelerator Driven Subcritical Assembly Facility Concept," Y. Gohar, I. Bolshinsky, H. Belch, D. Naberezhnev, T. Sofu, A. Talamo, and Z. Zhong, XX Intl. Workshop on Charged Particle Accelerators (IWCPA-2007), Alushta, Ukraine, September 9-15, 2007.
4. "Conceptual Design Configuration for Electron Accelerator Driven Subcritical Facility," H. Belch, Y. Gohar, T. Sofu, Z. Zhong, XX Intl. Workshop on Charged Particle Accelerators (IWCPA-2007), Alushta, Ukraine, September 9-15, 2007.
5. T. Sofu, et.al., "Thermal-Hydraulic Analysis of Electron Targets for Neutron Generation in a Subcritical System," Trans. Amer. Nucl. Soc. Annual Mtg., Reno, Nevada (June 4-8, 2006).
6. "Neutronic, Thermal-Hydraulic, and Structural Analysis of the Electron Target for an Accelerator-Driven Subcritical System," T. Sofu, Y. Gohar, H. Belch, D. Naberezhnev, and Z. Zhong, Eighth International Topical Meeting on Nuclear Applications and Utilization of Accelerators (AccApp'07), Pocatello, Idaho, July 30-August 2, 2007.
7. "Multi-Physics Analysis of an Electron Target for the KIPT Subcritical Assembly," T. Sofu, Y. Gohar, H. Belch, Z. Zhong, D. Naberezhnev, XX International Workshop on Charged Particle Accelerators (IWCPA-2007), Alushta, Ukraine, September 9-15, 2007.
8. MCNPX Version 2.5.0 User's Manual (LA-CP-05-0369) Los Alamos National Laboratory, (http://mcnpx.lanl.gov/) April 2005.
9. STAR-CD Version 3.26 User's Manual, (http://www.cd-adapco.com/products/STAR-CD/), CD-adapco, Melville, NY.
10. MSC NASTRAN and MARC User's Manual, (http://www.mscsoftware.com/), MSC Software Corporation, Santa Ana, CA.

Nuclear Engineering Division
Argonne National Laboratory
9700 South Cass Avenue, Bldg. 208
Argonne, IL 60439-4842

www.anl.gov

A U.S. Department of Energy laboratory managed by UChicago Argonne, LLC